Mon. Not. R. Astron. Soc. **000**, 1–20 (2008) Printed 26 July 2010 (MN LATEX style file v2.2)

Formation of terrestrial planet cores inside giant planet embryos.

Sergei Nayakshin
Department of Physics & Astronomy, University of Leicester, Leicester, LE1 7RH, UK

Accepted 2008 ?? ??. Received 2008 ?? ??; in original form 2008 05 ??

ABSTRACT
Giant planet embryos are believed to be spawned by gravitational instability in massive extended ($R \sim 100$ AU) protostellar discs. In a recent paper we have shown that dust can sediment inside the embryos, as argued earlier by Boss (1998) in a slightly different model. Here we study numerically the next stage of this process – the formation of a solid core. If conditions are conducive to solid core formation, the centre of the gas cloud goes through the following sequence of phases: (i) becomes grain (and metal) rich; (ii) forms a terrestrial mass solid core via a rapid collapse driven by self-gravity of the grains; (iii) starts to accrete a gaseous atmosphere when the solid core reaches mass of a few to $10\,\mathrm{M}_\oplus$. This sequence of events may build either terrestrial planet cores or metal rich giant planets inside the larger gas reservoir of the giant planet embryo. In a companion Letter we argue that tidal and irradiation effects from the parent star should disrupt the outer metal poor layers of the embryo, releasing nearly "ready to use" planets. We propose this as an alternative way to build planets.

Key words:

1 INTRODUCTION

It would be clearly an attractive proposition if planets could form in a way similar to stars, e.g., by gravitational contraction followed by a rapid collapse of gas or solid material clumps. A clear route to this is gravitational instability (GI) of the parent protoplanetary disc, when the latter fragments onto gaseous clumps with masses of a few Jupiter mass ($M_J = 10^{-3}\,\mathrm{M}_\odot$). Boss (1997) argued that giant planets may form this way. However giant planets in the Solar System contain massive solid cores, and they are also much more metal rich than the Sun. Thus a simple gravitational collapse of a giant planet embryo could not work. Boss (1998) suggested that solid cores of the order of a few Earth masses ($\mathrm{M}_\oplus \approx 3\times10^{-6}\,\mathrm{M}_\odot$) can be formed if dust grows and sediments inside the giant embryos. Boss et al. (2002) further suggested that even more massive and icy cores can be built inside giant proto-planets at 10 to a few tens of AU distances. These authors further pointed out that metalicity of such planets could be raised if gas envelopes of giant planet embryos are removed by photo-evaporation due to a nearby OB star. Such a model would account for both the solid cores and high metalicities of the giant planets.

However, Wuchterl et al. (2000) argued that giant planet embryos may become convective within the first $\sim$ 100 years of their evolution, and that convection may inhibit grain sedimentation. Helled et al. (2008); Helled & Schubert (2008) have recently confirmed this, obtaining much smaller solid cores than the model of Boss (1998) predicts. These authors also found that their model gas clumps either were too hot to begin with or became hot too soon for a significant dust growth, instead vaporising the grains.

Another objection to the gravitational instability model for planet formation was pointed out by Rafikov (2005) who showed analytically that the disc cannot even fragment on self-bound gas clumps inside $\sim$ 30 AU at least. The core accretion (CA) model for planet formation (e.g., Wetherill 1990; Pollack et al. 1996; Ida & Lin 2008) therefore seems more attractive to many.

However, the extrasolar planets observed at large ($R_p \sim$ 100 AU) separations from their parent stars (Baraffe et al. 2010) cannot be explained by the CA model due to exceedingly long core formation times. These planets were almost certainly formed by the gravitational disc instability (e.g., see simulations by Stamatellos & Whitworth 2008; Inutsuka et al. 2009; Machida et al. 2010; Rice et al. 2010).

Formation by GI is not absolutely forbidden even for the giant planets observed inside a few AU disc. True, the planets could not have started to form in situ there because initially giant embryos are much less dense than the local tidal density (see §2 below). However, radial migration of massive planets (Goldreich & Tremaine 1980) due to planet-disc torques is now an accepted ingredient of any planet formation theory, and provides an attractive explanation for the observed distribution of extrasolar planets in the radial range of $\sim 0.1 - 2.5$ AU (Armitage 2007), and

"hot jupiters" even closer in. We do not see why it is not possible for the giant planets to form at very large radii by GI and then migrate inwards to a few AU if they contract quickly enough. In a companion paper (Nayakshin 2010b; submitted to MNRAS, referred below as paper III) we argue that such a long-range migration is possible in the very early phase of formation of the parent star, when the disc mass is comparable to that of the star.

Furthermore, Boss et al, Wuchterl et al, and Helled and co-authors all considered embryos with gas densities of order 10^{-8} g cm^{-3} (perhaps having in mind the tidal density constraints for Jupiter at ~ 5 AU). Nayakshin (2010a, "paper I") showed the disc fragmentation constrains (Gammie 2001; Rice et al. 2005; Rafikov 2005) require that the initial density of gas clumps formed at ~ 100 AU from the star is around 10^{-13} g cm^{-3}. This fluffy initial state of giant embryos is also much cooler, with typical temperatures of only ~ 100 K, an order of magnitude lower than in the study by Helled an co-authors.

It is thus not surprising that we found in paper I such embryos to be much more promising sites of grain growth and sedimentation than did Helled et al. (2008); Helled & Schubert (2008). For reasonable opacity values, dust grows and sediments inside isolated giant planet embryos with masses between a few and $10-20$ Jupiter masses most readily. Since the embryos are approximately isentropic at birth, convection did not appear to be important in opposing grain sedimentation.

For technical reasons, the calculations were stopped in paper I when the grain density in the inner region of the gas clump reached that of the gas. In this paper we extend the calculations similar to those presented in paper I to later times. As predicted analytically in paper I, the inner region becomes completely grain-dominated by mass and then undergoes a rapid collapse. The gas component is "protected" against the collapse by the pressure gradient, and thus the two phases separate at the cloud centre. The grains form a high density "solid"' core (it is most likely melted or even liquid given the high energy release, but we shall still refer to it as a solid core as it may solidify later on when it cools).

Our main results can be summarised as following:

• The heat generated by the rapid assembly of the high-Z core produces a negative feedback on the core's growth. Grains can be melted, driven away convectively or by a bulk gas expansion, cutting off further core growth. Thus, concerning the final mass of the solid cores, our results are less optimistic than that of Boss (1998); Boss et al. (2002), but more optimistic than that of Helled et al. (2008); Helled & Schubert (2008). Continuing the trends from paper I, the embryos of a few to ten Jupiter masses usually yield the heaviest solid cores. More massive giant embryos are hotter to begin with and hence reach the grain vaporisation temperature sooner.

• Gas immediately adjacent to the solid core is strongly influenced by the energy release due to the core's assembly. Strong convection sets in (thus confirming its importance but only after the core formation), frequently supplemented by an outward gas expansion.

• Resolving the region near the solid core is challenging numerically, which implies that we probably underestimate the degree to which the gas becomes bound to the core. Even so, in a simulation where most of the giant embryo gets unbound, the solid core is left with a gas atmosphere of $\sim 0.03\,M_\oplus$. This shows that solid cores bred inside giant embryos may attract a gaseous atmosphere from within the embryo. This atmosphere is metal rich.

• We then use analytical arguments and a physical analogy to the classical results from the core accretion model for giant planet formation (e.g., Mizuno 1980; Pollack et al. 1996). We suggest that as the solid core mass increases above $\sim 10-20\,M_\oplus$, a runaway gas accretion sets in, in which the gas envelope collapses on itself. The resulting solid core plus a metal-rich self-bound atmosphere should be similar to a giant planet.

• In one of the simulations presented below most of the gas envelope gets unbound by the energy release from the core. This shows that, at least in the high optical depth cases, the heat released by the core's accretion may remove the envelope without an outside help. We believe that this outer layers blowout process may be even more prominent (e.g., likely) when the massive atmosphere collapse occurs, as that may release even more energy.

• We suggest that the outer metal-poor layers of the giant embryo could also be removed by physical collisions of embryos.

• We find that the protective giant embryo environment strongly diminishes the role of turbulence. We show that turbulent gas velocities would have to be as large as 0.3 times the sound speed to prevent gravitational collapse of the "grain sphere" into the solid core. As these high speeds are unlikely, we argue that solid cores can be built by a direct gravitational collapse inside the giant envelopes *without* having to go through the intermediate step of planetesimals. The planetesimals are thus not building blocks of planets in this picture. They are the material that did not join the core.

• Thus, in contrast to the classical planetesimal core assembly route (e.g., Safronov 1969; Weidenschilling 1980; Wetherill 1990), we would expect a far smaller fraction of the solid mass to be locked into intermediate (e.g., a km) size bodies.

• The main building blocks of solid cores in our scenario are pebble sized grains (e.g., ~ 10 cm). Grains of this size sediment efficiently enough and yet slowly enough as to avoid shattering in high speed collisions.

• Concluding, our key point is that the combination of dust sedimentation, solid core accretion and gas envelope collapse, on the one hand, with the removal of the outer metal-poor envelope of the embryo on the other, may result in terrestrial planet embryos, terrestrial planets, or giant planets, depending on when the envelope removal occurs.

In the follow-up paper already mentioned above (paper III), we argue that removal of the giant embryo by tidal shear from the star helped by heating caused by irradiation is un-escapable for giant planets migrating closer in than a few to a few ten AU. An exception to this could be a more massive giant planet $M_p \gtrsim 20 M_J$ that could undergo the "second collapse" (Larson 1969; Masunaga et al. 1998) before it is disrupted. Such massive planets should have metalicities close to that of their parent stars.

A hybrid regime of planet formation is possible, in which the solid cores are hatched inside the giant planet embryos,

delivered into the inner disc and left there when the embryos are disrupted. These solid cores may continue their growth by accumulation of solid material from the disc (rather than the parent embryo) in direct impacts, and then accrete massive gaseous envelopes from the surrounding gas disc, resulting in gas giant planets. In this case the beginning phase of planet formation is as in the modified GI hypothesis we study, but continuation as in the core accretion theory.

Future detailed calculations and comparison to observations are needed to test feasibility of these ideas. In any event it seems very clear that the gravitational instability model for planet formation has been discounted by most authors without a proper critical review of all the evidence.

2 PRELIMINARIES

2.1 Initial properties of self-gravitating clumps

In paper I we argued that the properties of the giant planet embryos formed by gravitational instability in the disc at their inception should be similar to that of the first cores of same mass. The key properties of first cores, taken from the results of Masunaga & Inutsuka (1999) as explained in paper I, are briefly reproduced here for reader's convenience. The opacity law is taken in the form

$$\kappa(T) = \kappa_0 \left(\frac{T}{10}\right)^{\alpha} , \tag{1}$$

where κ_0 is the opacity at $T = 10$ K, and reasonable values of α are thought to be between 1 and 2. For simplicity, in this paper we only consider the $\alpha = 1$ case (§3.5). The initial radius of the first core is given by

$$R_{\rm fc} = 6.0 \text{ AU } m_1^{-1/3} T_1^{\frac{1+4\alpha}{9}} \kappa_*^{4/9} , \tag{2}$$

where $\kappa_* = \kappa_0/0.01$ and $T_1 = T_{\rm init}/10$K is the initial gas temperature, e.g., the temperature of the parent gas material (the disc or the molecular cloud). Finally, $m_1 = M_{\rm fc}/10M_J$. The mean density of the first core is defined by

$$\rho_{\rm fc} = \frac{3M_{\rm fc}}{4\pi R_{\rm fc}^3} = 6.6 \times 10^{-12} \text{ g cm}^{-3} \, m_1^2 T_1^{-\frac{1+4\alpha}{3}} \kappa_*^{-4/3} , \tag{3}$$

The mean temperature of the first core is estimated as

$$T = \frac{1}{3} \frac{G M_{\rm fc} \mu}{k_B R_{\rm fc}} = 146 \text{ K } m_1^{4/3} T_1^{-\frac{1+4\alpha}{9}} \kappa_*^{-4/9} . \tag{4}$$

The cooling time of the first core is found to be

$$t_{\rm cool} = 380 \text{ years } m_1^{2/3} T_1^{-4/3} \kappa_*^{1/9} . \tag{5}$$

Note that the cooling time becomes longer with time, as the gas clump contracts and becomes optically thicker (paper I).

2.2 Dust sedimentation in isolated first cores

The calculations in paper I were done under the assumption that the first core gains or looses no mass from the surroundings. This limit applies if the mass exchange rate satisfies (for $\alpha = 1$) $|dM_{\rm fc}/dt| \ll 10^{-2} M_J \text{ yr}^{-1}$, which does depend on parameters of the first core (see paper I). We shall continue to assume this in the present paper as well, and hence the mass of the embryo is a free parameter of our calculations.

It was shown in paper I that grain sedimentation timescales can be shorter than the "vaporisation time", $t_{\rm vap}$, which is the time needed for the first core to heat up to the grain vaporisation temperature of about 1400 K. The calculations were stopped when the density of the dust was equal to that of the gas in the inner part of the cloud. Continuation of the calculations leads to the dust density increasing even further, and then a gravitational collapse. This then requires a treatment for the solid core forming in the innermost part of the gas cloud. Before we present calculations that now include formation of the cores, we first discuss the order of magnitude of physical characteristics of the solid cores.

2.3 Maximum masses of solid cores

The first question to ask about the solid cores built inside isolated first cores is how massive they could be. The total mass of "high-Z" elements, e.g., those excluding Hydrogen and Helium, is about

$$M_{\rm Z,t} = f_g M_{\rm fc} \approx 60 \, {\rm M}_\oplus \, \frac{f_g}{0.02} \, m_1 , \tag{6}$$

where $f_g = 0.02$ is the metal mass fraction (0.02 for gas of Solar metalicity). This mass includes ices and organics that are probably too volatile to contribute to the solid core, as the surrounding gas temperature is typically around 1000 K. The mass of refractory material (e.g., silicates) that can be used to build a massive core is hence expected to be about $\sim 1/3$ of the total heavy elements mass. Therefore, the maximum mass of the solid core that can be built inside an *isolated* first core is

$$M_{\rm Z,c} = \frac{1}{3} f_g M_{\rm fc} \approx 20 \, {\rm M}_\oplus \, \frac{f_g}{0.02} \, m_1 , \tag{7}$$

The minimum core mass (same as the opacity fragmentation limit Low & Lynden-Bell 1976; Rees 1976) is a few Jupiter masses, and the maximum mass that permits grain sedimentation is typically a few tens of M_J. Accordingly, the total mass of useful core-building material is expected to be in the range of ~ 7 to ~ 60 or so Earth's masses. These estimates should be tripled if the embryo is cool enough to permit formation of ices.

2.4 Binding energy of solid cores

We expect the core of high-Z elements to have a density of the order of the terrestrial planet densities, e.g., $\rho_c \sim$ a few g cm^{-3}. The corresponding radial size of the solid core, $R_{\rm core} = (3M_c/4\pi\rho_c)^{1/3}$, is in the range of 10^8 to a few times 10^9 cm, which is about 5 orders of magnitude smaller than the size of the first core. The binding energy of the solid core is

$$E_{\rm bind,c} = \frac{3}{5} \frac{G M_{\rm core}^2}{R_{\rm core}} = 1.3 \times 10^{39} \text{ erg } \left(\frac{M_{\rm c}}{{\rm M}_\oplus}\right)^{5/3} \rho_c^{-1/3} . \tag{8}$$

The binding energy of the first core at formation is in the rough range of 10^{40} to 10^{42} erg (see paper I), and it increases in proportion to the virial temperature of the core (dimensionless $\tilde{T}(t)$ introduced in paper I) as the core contracts. Hence a massive enough solid core, $M_p \sim 10 \, {\rm M}_\oplus$, may release an amount of energy comparable to the binding energy

of the core itself, strongly affecting the core. Furthermore, for a constant density gas sphere, inside the embryo, the binding energy scales as $M^2(R)/R \propto R^5$, and the thermal energy scales as $M(R) \propto R^3$. Thus building up a massive solid core is very likely to heat up the gas at least in the inner parts of the first core.

3 NUMERICAL METHOD

3.1 Overall approach

We use the same set up, equations and numerical techniques as in paper I, adding to the code several new features to describe the evolution of the solid core and its effects on the surrounding gas. In brief, spherically symmetric Lagrangian coordinates are used. A cell is defined by its fixed gas mass, whereas the radial position of the shell changes as the gas contracts or expands. The equations are those widely used in stellar evolution calculations, except we employ a time-dependent approach that does not assume the hydrostatic or the energy balances for the gas. We find that this time-dependent approach is very important for the problem at hand. Both the grain and the gas distributions may evolve very rapidly when a heavy-Z core is formed via a rapid (and hence quite luminous) accretion of grains.

The grains are described as a second fluid that is under the influence of gravity and gas drag. Grains are allowed to slip through the gas, e.g., from one gas radial shell into the neighbouring one. For example, grains can move from an outer into an inner radial shell when they sediment, or be carried in the opposite direction by turbulent or convective mixing.

3.2 Convection and grain convective mixing

The transport of energy is primarily due to the classical radiation diffusion flux, although convective flux does become important during certain stages of the evolution, e.g., when the liquid core's luminosity is high. The mixing length theory for convection is used (e.g., §7 in Kippenhahn & Weigert 1990). We impose an upper limit to the convective flux, $F_{\rm con}$, given by $F_{\rm c,max} = c_s P$, where c_s and P are the gas sound speed and pressure, respectively.

In contrast to paper I, the convective motions of the gas are allowed to contribute to mixing of grains, impeding grain sedimentation. Treating this process as a diffusion process, similar to the turbulent mixing (paper I and Fromang & Papaloizou 2006), we "add" the convective mixing to turbulent mixing by increasing the turbulent mixing coefficient α_d introduced in paper I:

$$\alpha_d' = \alpha_d + \frac{F_{\rm con}}{F_{\rm c,max}} \ . \tag{9}$$

This prescription is motivated by the fact that the convective mixing length by definition becomes about equal to the gas pressure scale-height, e.g., the radius of the first core, $R_{\rm fc}$, when $F_{\rm con} = F_{\rm c,max}$. Note that the maximum of $\alpha_d' \approx 1$. Strong convective motions could therefore be quite important in opposing and perhaps even reversing grain sedimentation, but we find that this fortuitously occurs "too late", when a massive solid core has already formed (see §4 below for an example).

3.3 The inner grain boundary: a heavy elements core

Like previous authors (e.g., Helled et al. 2008), we found it very challenging numerically to resolve the radial scales of the heavy-Z core for the entire duration of the simulations. As there is very little gas mass on these scales, except if and when a massive gas atmosphere builds up, many more radial shells are needed. These shells require tiny time steps despite being not very interesting for most of the calculation. Therefore, due to numerical constrains, the length scales that we do resolve for most of the simulations are still large compared with the solid core, of the order of $\sim 10^{11}$ cm. Note that a snapshot re-simulation can of course be done at a higher resolution if one is interested in the small scale structure.

Given that the smallest scales are not properly resolved, there is an uncertainty in choosing the boundary conditions for grains at $R = 0$ radius, that is in the very first *gas* mass zone. In paper I we assumed that the grains in the innermost zone are suspended by turbulent mixing *until* the grain density in the zone exceeded that of the gas. Presumably the inverse drag effects imposed by grains on the gas stifle the turbulence once the grains dominate the gas by mass. We stopped the simulations at that moment in paper I, delaying a study of core accretion to this paper.

There is no a priory reason why turbulent mixing must be effective at $R \to 0$. If it vanishes in that region, then grains may start to sediment into a high-Z core even before they overwhelm the gas by mass in the first zone. Helled et al. (2008) classified a similar approach as "case 1", whereas not introducing a solid core until the grains dominate the central zone is is analogous to their case 2. However, numerical experiments that we did showed that the difference in results between these two cases is minor for most of the interesting parameter space. Namely, we found that before the first zone is dominated by grains, the high-Z core grows very slowly in "case 1" anyway. This is due to two factors. First of all, the grain density in the central zone is small during these "early" times. Secondly, the grains are themselves small, yielding a rather small sedimentation rate.

In the simulations we explored, there is a period of a very rapid (but limited) growth of the solid core in both case 1 and 2. The only significant difference arises for rapidly contracting first cores that reach grain vaporisation temperatures before the rapid high-Z core growth phase. In case 1, a small high-Z core may be built, whereas it is completely absent in case 2. We shall keep this fact in mind, and proceed to use only the case 1 in this paper, since it turned out to be numerically more stable during the episodes of the rapid high-Z core growth. This does not lead to any loss of generality of our results. We still cover the appropriate parameter space of the problem while avoiding presentation of minor differences from very similar runs.

Therefore, our prescription for the core accretion rate is

$$\frac{dM_{\rm core}}{dt} = \begin{cases} M_{d,1}(u_2 - u_{a2})/R_{g2} & \text{if } \ u_2 - u_{a2} > 0 \\ 0 \quad \text{otherwise} \ . \end{cases} \tag{10}$$

where $M_{d,1}$ is the mass of the dust in the first gas zone, R_2 is the outer radius of the first gas zone, and $(u_2 - u_{a2})$ is the velocity with which grains arrive into the first zone from the second gas zone. For simplicity, we assume that the core

has the same material density as the grains, ρ_a. Therefore, the outer radius of the core is $R_{\rm core} = (3M_{\rm core}/4\pi\rho_a)^{1/3}$. This radius becomes the new inner boundary for the gas: as the core builds up, the inner radius of the first Lagrangian mass zone becomes $R_1 = R_{\rm core}$. As the radius of the heavy elements core is initially orders of magnitude smaller than R_2 this does not lead to any significant perturbations for the gas.

3.4 Radiation from the forming core

Accretion of grains onto the surface of the solid core generates accretion luminosity equal to

$$L_{\rm acc} = \frac{dE_{\rm bind,c}}{dt} = \frac{GM_{\rm core}\dot{M}_{\rm core}}{R_{\rm core}} \ . \quad (11)$$

The radiative flux boundary condition is modified from the zero flux one used in paper I, to read

$$F_{\rm rad}(R_1) = \frac{L_{\rm core}}{4\pi R_1^2} \ . \quad (12)$$

3.5 Fiducial parameters

The outcome of our grain sedimentation calculations depend on many parameters, such as: the initial grain size a_0; grain mass fraction relative to gas, f_g; turbulent mixing coefficient α_d; maximum velocity $v_{\rm max}$ for grain growth; the opacity power law index α; the opacity coefficient κ_0; the mass of the first core, $M_{\rm fc}$; and the initial (same as ambient) gas temperature $T_{\rm init}$. The parameter space is too large to explore completely in one paper.

Fortunately, we find that some of the parameters listed above change the end results very little except near regions delineating critical behaviour changes. For example, the initial grain size is irrelevant in most cases as small grains grow very quickly in our prescription due to Brownian motions. Grains also evaporate very quickly once gas temperature exceeds $T_{\rm vap} \sim 1400$ K, and so their size is not crucial in this case as well. Only when the other parameters of the problems are such that the grain growth time, $t_{\rm gr}$, is about the vaporisation time, $t_{\rm vap}$ (see paper I), the exact initial value of a_0 is important.

We also find that there is a degeneracy in the role of some of the parameters. As the interior temperatures of the first cores are typically of order of 1000 K, the typical opacity of the first core is $\kappa \sim \kappa_0 10^{2\alpha}$. A larger value of α can be compensated for by a smaller value of κ_0 to yield a similar opacity through the first core, although there may still be important differences between these cases near the high-Z core or on the outskirts of the first core.

We shall therefore fix some of the less influential parameters at "reasonable" values, motivated by observations whenever possible, and also try to avoid model degeneracies. In line with this, we set $f_g = 0.02$, $T_{\rm init} = 10$ K, $\alpha = 1$, $a_0 = 1$ cm, $v_{\rm max} = 1$ m s^{-1}. A logarithmic gas mass grid is used, so that the mass of grid cell increases with index i as $\Delta M_{i+1} = 1.08\Delta M_i$, where $i = 1, 2, ..., i_{max}$. We used $i_{max} = 170$ cells for most of the runs below, which results in the mass of the innermost gas cell of $\sim 10^{-3}\,{\rm M}_\oplus$ for $M_{\rm fc} = 10M_J$.

This leaves three parameters that we found to be instrumental in determining the outcome of the calculations, and we shall vary these in a relatively broad range: the opacity coefficient κ_0, the mass of the first core, $M_{\rm fc}$, and the turbulent mixing coefficient, α_d.

3.6 Simulations Table

The parameters of the simulations selected for presentation in this paper, and some of the more important results of these simulations are listed in Table 1. The first column is the simulation "ID", which starts with a letter M, H or L. These stand to indicate the mass of the first core: "H" for heavy, $M_{\rm fc} = 20M_J$; "M" for medium, $M_{\rm fc} = 10M_J$; and "L" for light, $M_{\rm fc} = 5M_J$. The digit next to the first letter refers to the opacity coefficient κ_0 of the simulation, such that J_k satisfies $J_k = -\log_{10}\kappa_0$. For example, $\kappa_0 = 0.01$ will have $J_k = 2$ in its ID. Similarly, the symbol α followed by a digit J_α signifies the magnitude of the turbulent viscosity coefficient, α_d, so that $J_\alpha = -\log_{10}\alpha_d$.

The results part of Table 1 starts with two columns for two time variables, $t_{\rm end}$ and $t_{\rm acc}$, both in units of 10^3 years. The former is the duration of the simulation. The simulations were run for as long as there were an appreciable change in the results or until the simulations stalled due to a vanishingly small time step. The latter time entry, $t_{\rm acc}$, is the time of the "runaway solid core accretion phase". The "-" symbol in this column indicates that the simulation never entered this phase because grains vaporised earlier than they sedimented. The "NA" (not applicable) entry refers to the cases when the core accretion is very gradual, so that no runaway phase can be defined. This happens when turbulent mixing is significant.

The last three columns in the Table relate to the masses of the first cores in units of Earth masses. $M_{\rm core}$ is the final mass of the core, while M_{c1} and M_{c2} are its masses at two intermediate times, $t = 2 \times 10^3$ and $t = 10^4$ years, respectively. These two masses are given to indicate the speed with which the cores are assembled.

4 10 M$_{\rm J}$ FIRST CORES

Here we present several calculations for first cores with mass of $10M_J$. IDs of these runs start with letter "M" in Table 1. We shall first look at several tests with the same level of turbulent mixing parameter, $\alpha = 10^{-3}$, labelled $\alpha 3$ in Table 1.

4.1 Medium-high opacity case (M1α3)

We start with a relatively high opacity case, $\kappa_0 = 0.1$. At the typical first core's interior's temperature, we have $\kappa(T = 10^3{\rm K}) = 10$ for this particular choice of κ_0. This is quite high but may well be reasonable at least in the innermost parts of the first core when dust sediments there.

Figure 1 shows the evolution of several key quantities as a function of time for this calculation. The solid and dotted curves in the upper panel of the figure show the grain size, a, and central gas density, ρ, in units of 10^{-9} g cm^{-3}, respectively. The dashed curve is the central gas temperature in units of 100 K. The solid curve in the lower panel

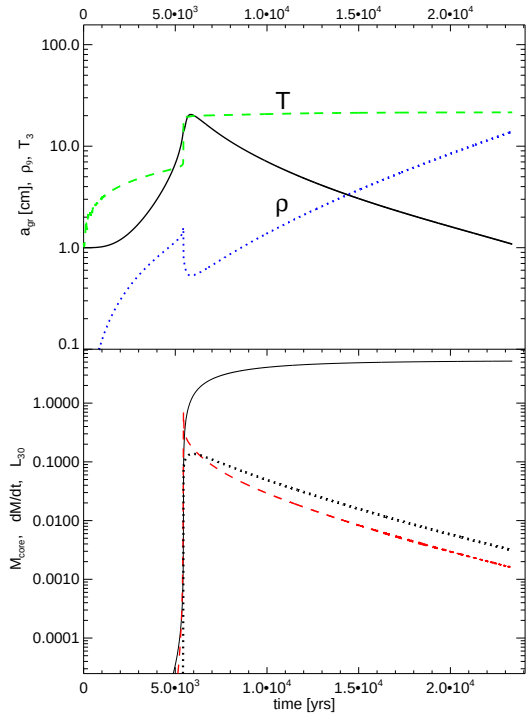

Figure 1. Results of simulation M1α3 (see §4.1 and Table 1). Upper panel: Grain size a in cm (black solid curve), dust-averaged temperature T_m (dashed green) in units of 10^3 K, central gas density in units of 10^{-9} g cm^{-3} (blue dotted). Lower panel: mass of the high-Z elements core, in Earth's masses (black solid), core's accretion rate in 10^{-2} M$_\oplus$ yr^{-1} (red dashed), and core's accretion luminosity in 10^{30} erg s^{-1} (black dotted).

shows the mass of the high-Z core in units of Earth's mass, whereas the dotted and the dashed curves show the core's luminosity (in 10^{30} erg s^{-1}) and accretion rate, in 10^{-2} M$_\oplus$ yr^{-1}.

The first $\sim 5 \times 10^3$ yrs of the simulation are familiar from paper I. The grains must grow to ~ 10 cm size before a significant dust sedimentation takes place. The evolution after that is marked by two stages: the "runaway" stage during which the high-Z core grows very rapidly, almost vertically in Figure 1, and the saturated growth stage when the accretion rate, core's luminosity and grain size all drop with time. This second stage is a testament to importance of feedback effects during the core's growth. This can be deduced by noting the abrupt central temperature increase at the end of the "runaway phase", when both the high-Z core mass and luminosity increase sharply, and the corresponding central gas density decrease. The temperature increase disrupts the hydrostatic balance in the central regions, causing an outward gas expansion.

These effects are seen in Figure 2 that presents the radial structure of the first core and the grain density distribution during and just after the end of the runaway core growth phase. The panels show the gas and the grain densities, the gas temperature, the radiative (black curves) and the convective luminosities (blue curves), and the gas (black) and the grain (red) radial velocities. The convective luminosity is defined by $L_{\rm con} = 4\pi R^2 F_{\rm con}$.

The first snapshot in figure 2, shown with the solid curves, corresponds to the time when the grain density in the inner region is equal to that of the gas, which corresponds to when we stopped the simulations in paper I. The mass of the high-Z core is only $\sim 3 \times 10^{-4}$ M$_\oplus$ at that point. As the grain density overtakes the gas density, the gas drag and turbulent mixing resistance to grain sedimentation rapidly weaken. This is seen in the inner part of the radial velocity curves sequence. As the inner part of the "grain sphere" contracts due to its own self-gravity, the accretion rate onto the high-Z core increases by orders of magnitude. The luminosity of the solid core shoots up to about a tenth of that produced by the whole first core (see the dashed and the dot-dashed curves in the upper right panel of the figure).

The heat produced by the build up of the high-Z core strongly affects the inner region of the cloud, heating up the gas there. The increased gas pressure initiates a rarefaction wave that moves gas outward, as can be seen in both the density and the velocity curves. It is likely that the grain sedimentation would continue at this stage if it were not for the gas entropy profile becoming strongly unstable to convection. The convective flux builds up to its maximum $F_{\rm c,max}$ value allowed (blue curves in the upper right panel) in the inner part of the cloud. Strong convective mixing drives some grains in the inner region outwards (see the red velocity curves for grains). Note a very good correlation in the positions of the peak of gain velocity curves in the inner part of the embryo with the maximum in the convection luminosity. This confirms that the outward motion of grains is driven by convection in this region.

The second, also quite important way in which the high-Z core growth self-regulates is vaporisation of grains. As the inner region of the computational domain heats up, grain growth and evaporation start to compete with each other. In fact the grain size decreases with time (upper panel in fig. 1), although not particularly rapidly in this simulation.

The existence of the two ways in which the high-Z cores can affect their surroundings and hence limit the rate of their own growth suggests that this feedback loop is quite robust qualitatively, despite quantitatively depending on details of the gas-grain interaction prescriptions and the parameter values.

These feedback effects preclude incorporation of all of the available condensible material in the high-Z core. Indeed, as much as ~ 20 M$_\oplus$ of such material is present in the first core, but only a quarter of it gets locked into the high-Z core. Clearly this result must be sensitive to the opacity of the first core, as lower opacity would allow more heat to escape the gas cloud, perhaps reducing the feedback effects.

4.2 Medium opacity case

We now present calculation M2α3 which is identical to M1α3 except the opacity is reduced to $\kappa_0 = 0.01$. The resulting evolution of the first core and the grain distribution is shown in Figure 3. Confirming the earlier made claim that embryo opacity is a key parameter of the problem, the resulting change in the dust sedimentation outcome is significant. As the cooling time of the first core decreases as κ_0 decreases, the cloud contracts more rapidly. Higher gas

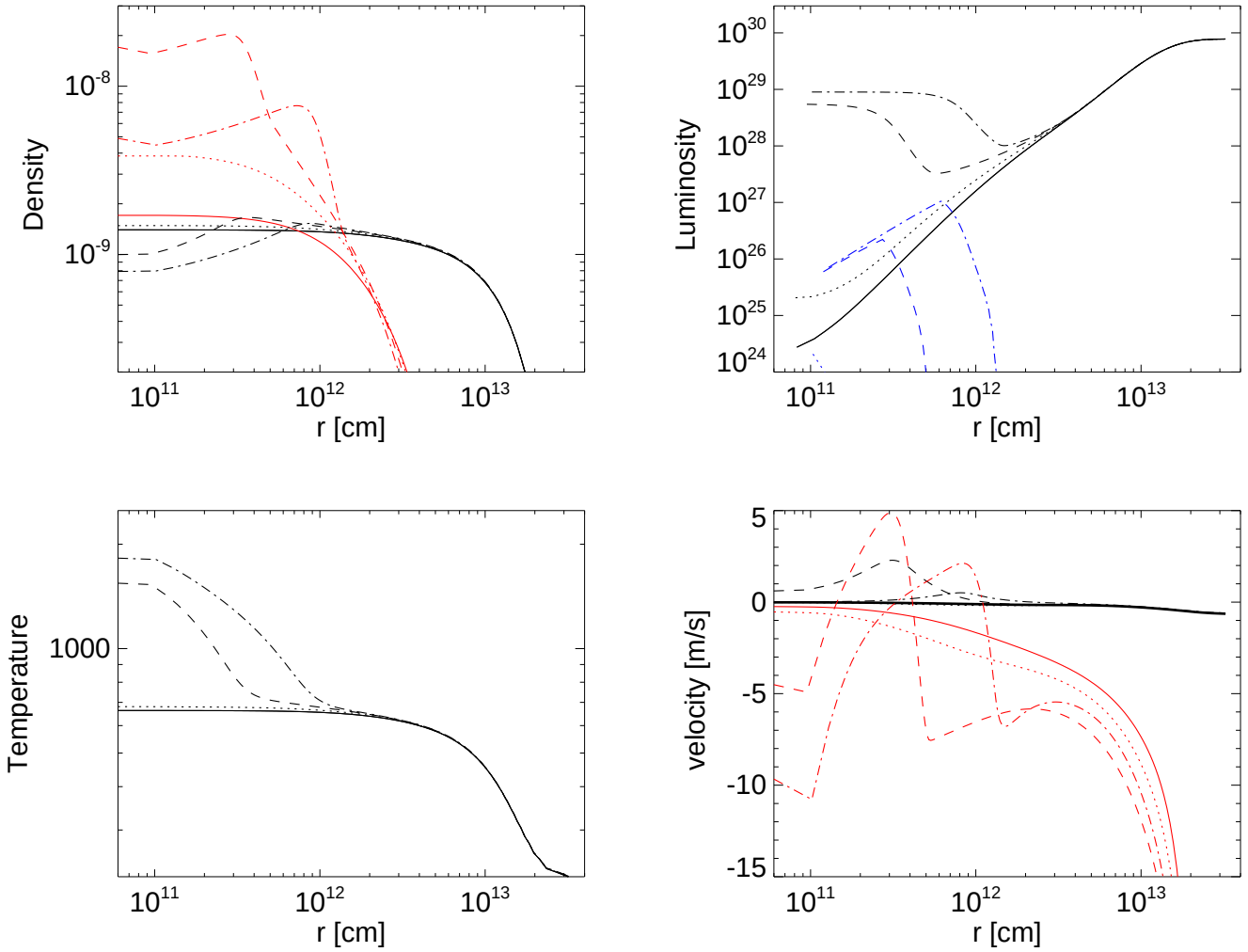

Figure 2. Radial structure of the first core during and just after the "runaway growth phase" in the simulation M1α3 (see Fig. 1). Densities and velocities of gas and grains are shown with the black and red curves, respectively. The different style lines are for times $t = 5386, 5417, 5446$ and 5469 years, for the solid, dotted, dashed and dash-dotted curves, respectively. The blue curves in the right upper panel show the convective luminosity which becomes relatively large after the high-Z core creation.

density promotes faster grain growth. Therefore, grains increase in size and sediment sooner in M2α3 than they did in simulation M1α3. The runaway accretion phase begins earlier, at around 2×10^3 years. As the core accretion rate is higher, the feedback effects of the growing high-Z core are more pronounced, and hence the rapid growth of the core saturates at a lower core mass, and a lower luminosity (cf. the lower panels of figures 1 and 3). As in simulation M1α3, the gas temperature near the core is above vaporisation temperature for the grains, causing grain melting and hence a plunge in the value of a at the peak of the runaway growth phase. In comparison to M1α3, reduced opacity enables the gas near the core to transfer the heat outward more rapidly. This allows a further density and temperature increase near the core, evaporating the grains further. A complete grain evaporation occurs at about 3,500 years in this calculation. Grain accretion onto the high-Z core then ceases, allowing the gas near the core to cool slightly. The contraction and the respective heating of the gas near the core continues. This stops any further core re-growth.

The final mass of the high-Z core in this simulation is $M_{\rm core} = 0.9996\,{\rm M}_\oplus$. The fact that it so close to the Earth's mass is of course a complete coincidence. Degrading the numerical resolution from $i_{max} = 170$ to $i_{max} = 140$, and repeating the simulation M2α3 leads to qualitatively very similar results but the final core mass is $M_{\rm core} = 1.24\,{\rm M}_\oplus$. This implies that higher numerical resolution calculations would yield somewhat lower masses for the final $M_{\rm core}$, but probably not by more than a factor of 2. This is acceptable to us given large uncertainties in parameter values. The decrease in the final core mass with an increasing resolution is probably due to feedback effects becoming even more pronounced as regions closer and closer to the core are resolved. We shall investigate these issues further in the future.

Figure 4 shows the radial structure of the first cores at and immediately after the runaway accretion phase for the simulation M2α3. There are many features similar to those

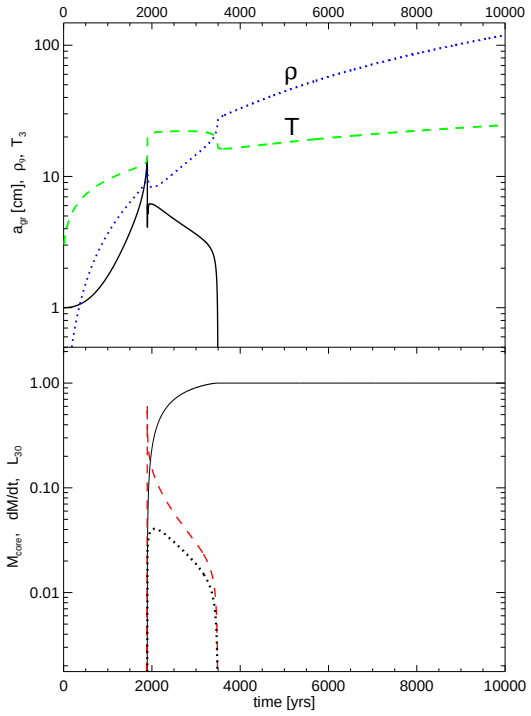

Figure 3. Same as figure 1 but for simulation M2α3. Note the anti-correlation between the size of grains and the central temperature after the high-Z core is created. This is due to a feedback loop: grains power core's accretion luminosity that heats up the central region of the first core, but the grains can then be melted by if the gas becomes too hot.

seen earlier in figure 2. Note a slightly lower core luminosity, which is in line with the lower final core mass. It is also interesting that the general grain sedimentation trend is reversed at "large" R, $R \sim 2 \times 10^{12}$ cm, as grains there start to move outwards (see the lower right panel in figure 4). This is caused by a rapid decrease (by a factor of two) in the grain size at the runaway accretion phase. The reduced size of grains implies a smaller sedimentation velocity, and sedimentation is apparently overpowered by turbulent mixing at these radii. The effect however does not last for long as grains re-grow and sedimentation continues.

4.3 Low opacity case

Simulation M3α3 probes the case of a yet smaller opacity, $\kappa = 0.001$. The cooling time of the first core in this case is very short. Therefore, the results of this test are "uninteresting" – grains grow to $a \approx 1.5$ cm only to be evaporated at about $t \approx 200$ years. We present no figures for this calculation. Shortly after the grains evaporate, the gas temperature approaches 2000 K, and the first core should undergo the second collapse (Masunaga & Inutsuka 2000) and probably form a giant planet mass object without a solid core.

4.4 Very high opacity

Simulation M0α3 is the highest opacity case we consider here, with $\kappa_0 = 1$. As the cooling time is very long for this simulation, the first core does not contract very much before the grains sediment into the high-Z core. The central density of the first core is much smaller than in the previously investigated cases, and for this reason it is plotted in units of 10^{-12} g cm^{-3} in Figure 5. As can be seen from the figure, the simulation M0α3 is very different from the lower opacity cases studied so far. The central temperature of the first core in M0α3 never becomes high enough to evaporate the grains, except at the very end of the simulation. This is why the grain size (solid curve in the upper panel of figure 5) and the accretion rate onto the solid core (red dashed curve in the lower panel of the figure) keep increasing through and after the runaway accretion phase, whereas in M1α3 and M2α3 these quantities peaked during the runaway phase and subsequently dropped with time.

Due to lower gas temperatures, the melting type of feedback does not take place in M0α3 before $t \sim 3 \times 10^4$ yrs. Grains continue to sediment and build up the central solid core at an increasing rate. The heat released by the core is trapped near the core due to a higher opacity of the embryo. The only way for the gas in the inner part of the first core to absorb the energy released by the high-Z core is to put it into a kinetic form. This drives a strong outward expansion.

Figure 6 shows the radial structure of the first core near the beginning of the high-Z core runaway accretion phase (solid curves) at $t = 8.5 \times 10^3$ yrs, and at a later time, $t = 2.44 \times 10^4$ yrs (dotted curves). Note an immense change in the luminosity curves (upper right panel of the figure). While initially heat production was all due to the compressional heating of the gas, at later times the energy production is dominated by the grain accretion onto the high-Z core. The innermost region of the gas becomes unstable to convection, and the convection flux then increases to the maximum sonic value that we impose (§3.2). At the same time, the convection flux is still very small compared with the radiative flux.

The increased luminosity of the high-Z core also forces the inner regions of the gas to become much hotter, although not as hot as to evaporate the grains (see the lower left panel of figure 6). The rarefaction in the inner $\sim 10^{12}$ cm of the first core is significant, e.g., gas density decreases by a factor of a few. Note that the motion of the gas and the increased convective grain mixing does cause some outward radial motion of the grains, although the innermost grain-dominated region becomes depleted mainly due to grain accretion onto the high-Z core (see the red curves in the upper left panel of the figure).

Further evolution of the first core is marked by a continuing energy release from the solid core, which continues to inflate the hot bubble within the first core until it actually breaks out – unbinds most of the gas in the outer parts of the first core. This can be seen in Figure 7, which presents the radial structure at time $t = 3.16 \times 10^4$ yrs. Note the very high temperature and density at small radii and, on the contrary, very low densities and a fixed temperature of 20 K at large radii. The latter is the minimum temperature imposed at the outer boundary for this simulation (and for most others; normally this plays no role at all as the tem-

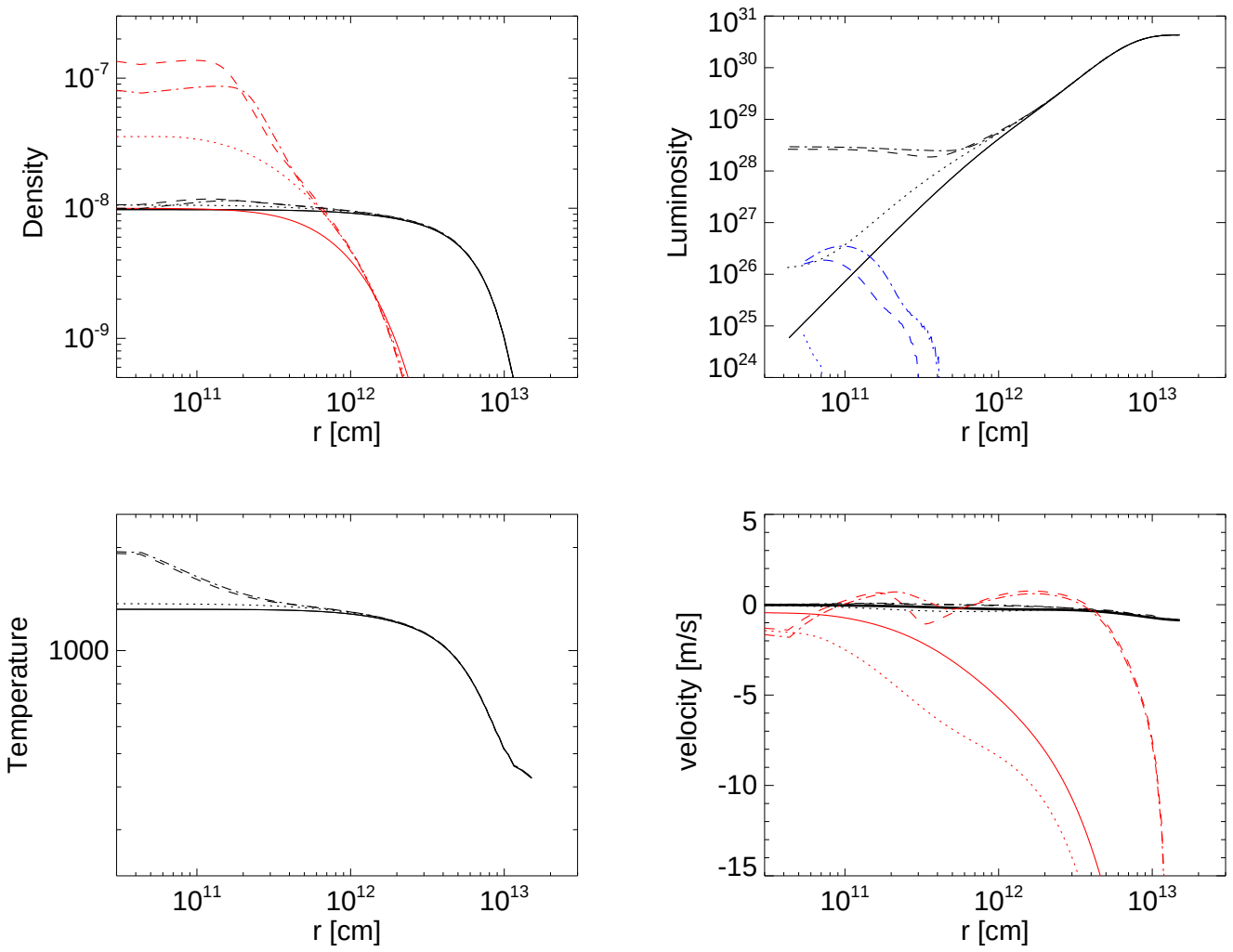

Figure 4. Same as figure 2 but for simulation M2α3 (see also figure 3). The snapshot times are $t = 1880$, 1892, 1902 and 1912 years.

perature of the outermost zone is usually higher than 20 K). The radial structure of the gaseous part of the first core in figure 7 can be divided into three parts : (i) the dense and hot envelope tightly bound to the high-Z core; (ii) the intermediate region at $10^{12} \lesssim R \lesssim 10^{13.5}$ cm; and (iii) the outer isothermal expanding shell. The last part of the fist core is the most massive one; it is completely unbound and is lost to the environment.

On the other hand, the region near the high-Z core can be called its atmosphere as it is apparently bound to the core. It is likely that the removal of the outer massive shell of gas actually promoted formation of the atmosphere by letting the heat escape the inner region more easily. The atmosphere is not massive at all: the upper left panel of figure 7 shows that it is around $\sim 0.03\,\mathrm{M}_\oplus$, compared with the mass of the core, $M_{\rm core} \sim 20\,\mathrm{M}_\oplus$. Nevertheless, it is important as it indicates that the solid cores formed inside the first cores can actually build up gaseous atmospheres if right conditions exist.

4.5 Nonlinear effects of turbulent mixing

We found that the models can be surprisingly and non-monotonically sensitive to the turbulent mixing parameter α_d. Simulations M2α2 and M2α4 are identical to M2α3 except that $\alpha_d = 10^{-2}$ and 10^{-4}, respectively. The evolution of the first core properties of simulation M2α2 and M2α4 is plotted in Figure 8, the left and the right panels, respectively.

Concentrating first on M2α2, we observe that its outcome is drastically different from that seen in figure 3. The larger turbulent mixing delays grain sedimentation by only about 50% (see $t_{\rm acc}$ in Table 1), but the gas in the first core is hotter by this time. Importantly, the gas temperature is now closer to the vaporisation temperature. As is clear from the upper panel of figure 8a, accretion luminosity of high-Z core is only $\sim 10^{27}$ erg s^{-1}, butthis is sufficient to push the gas near the core over the vaporisation temperature threshold. The grains evaporate rapidly soon after this, and a further growth of the high-Z core turns out impossible. The final mass of the core is $M_{\rm core} = 0.08\,\mathrm{M}_\oplus$. Note also that the

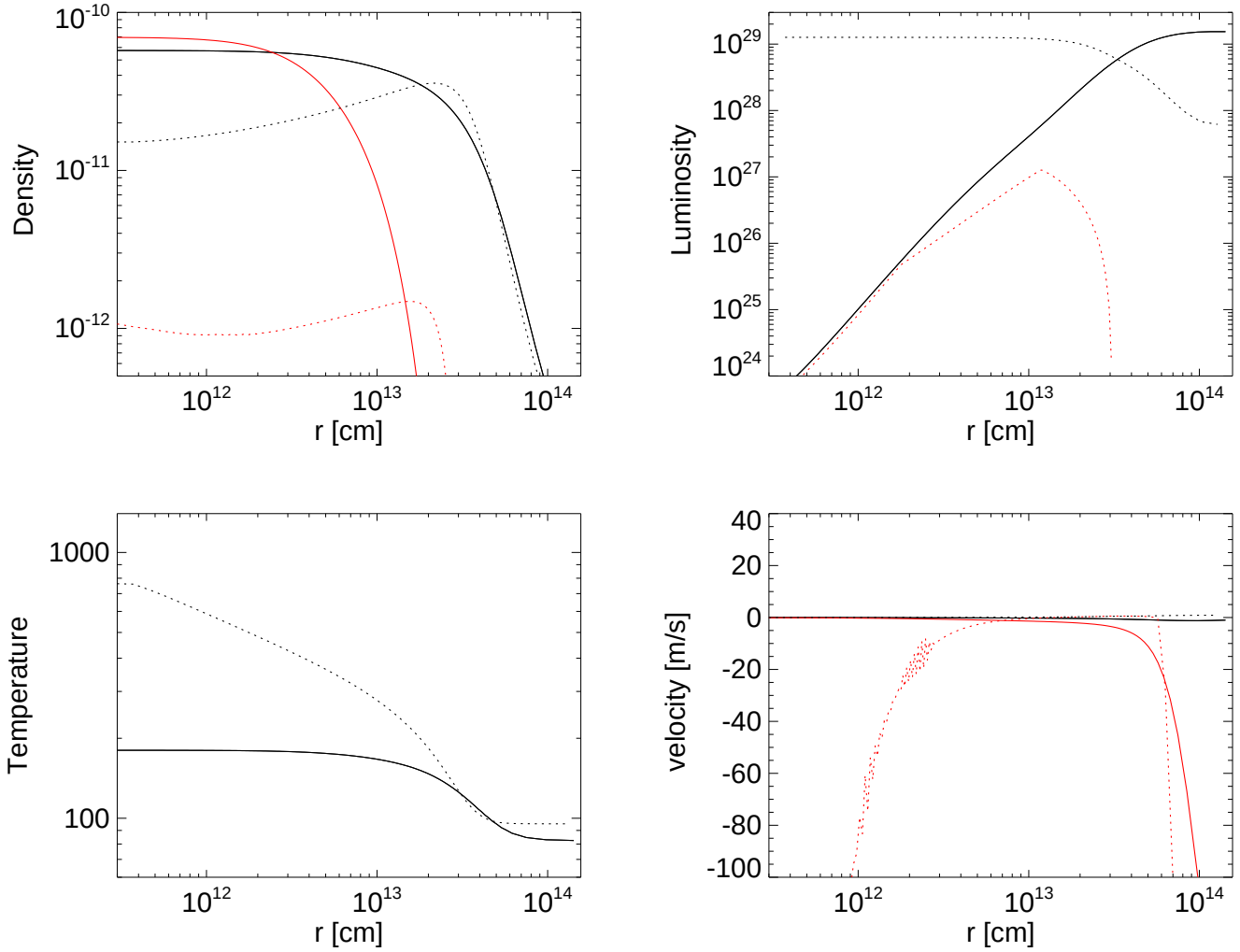

Figure 6. The radial structure of the first core near the end of simulation M0α3 (see Fig. 5). The solid and the dotted curves correspond to times $t = 8.5 \times 10^3$ and $t = 2.44 \times 10^4$ yrs, respectively. The red dotted curve in the top right panel shows the convective flux, saturated at the sonic value in the innermost part of the first core.

accretion rate of grains on to the high-Z core is smaller in M2α2.

The simulation M2α4 has a much lower level of turbulent mixing. Recalling the trend from M2α2 to M2α3, e.g., the increasing mass of the solid core with the decreasing turbulence parameter, one could expect the solid core to be more massive in M2α4 than that in M2α3 ($1\,M_\oplus$). However, the result is actually $M_{\rm core} \sim 0.7\,M_\odot$. The right panel of Figure 8 shows that the time evolution of the central part of the cloud in this simulation is quite complex. The maximum core accretion luminosity in this simulation actually exceeds that in M2α3 (compare the sharp red spikes in the luminosity curves for these two simulations). The energy released by the core then melts the grains rapidly. While in M2α3 grain re-growth occured almost immediately after the accretion luminosity drops, in M2α4 the gas near the core is a little hotter and hence the grains remain small for several hundred years. After the excess heat finally leaves the central region, grain growth restarts. This apparently leads to a second major core accretion episode at around 2200 years. The intricate feedback loop steps in again, melting the grains somewhat, but this time to the size of about 1 cm rather than ~ 0.1 cm. The grains are eventually vaporised at time $t = 3300$ years, very similarly to the simulation M2α3. The core mass is then frozen at the final value of $0.7\,M_\oplus$.

Comparing the three simulations, it appears that the role of the turbulent mixing is to smooth out the evolution of the grain size and the core accretion rate. Indeed, we note that turbulent grain mixing, in prescription we are using, may have both a negative and a positive effect on the solid core growth. Prior to the formation of a relatively massive core, turbulent mixing works only in one direction, that is opposing grain sedimentation. However, once a sufficiently massive core forms, gravity in the inner regions become dominated by the solid core itself rather than by the gas. The sedimentation velocity of the grains then increases above the "pre-core" theoretical value (paper I). The inner few zones of the core are then quickly emptied of the grain material by accretion onto the solid core. This has the effect of creating a

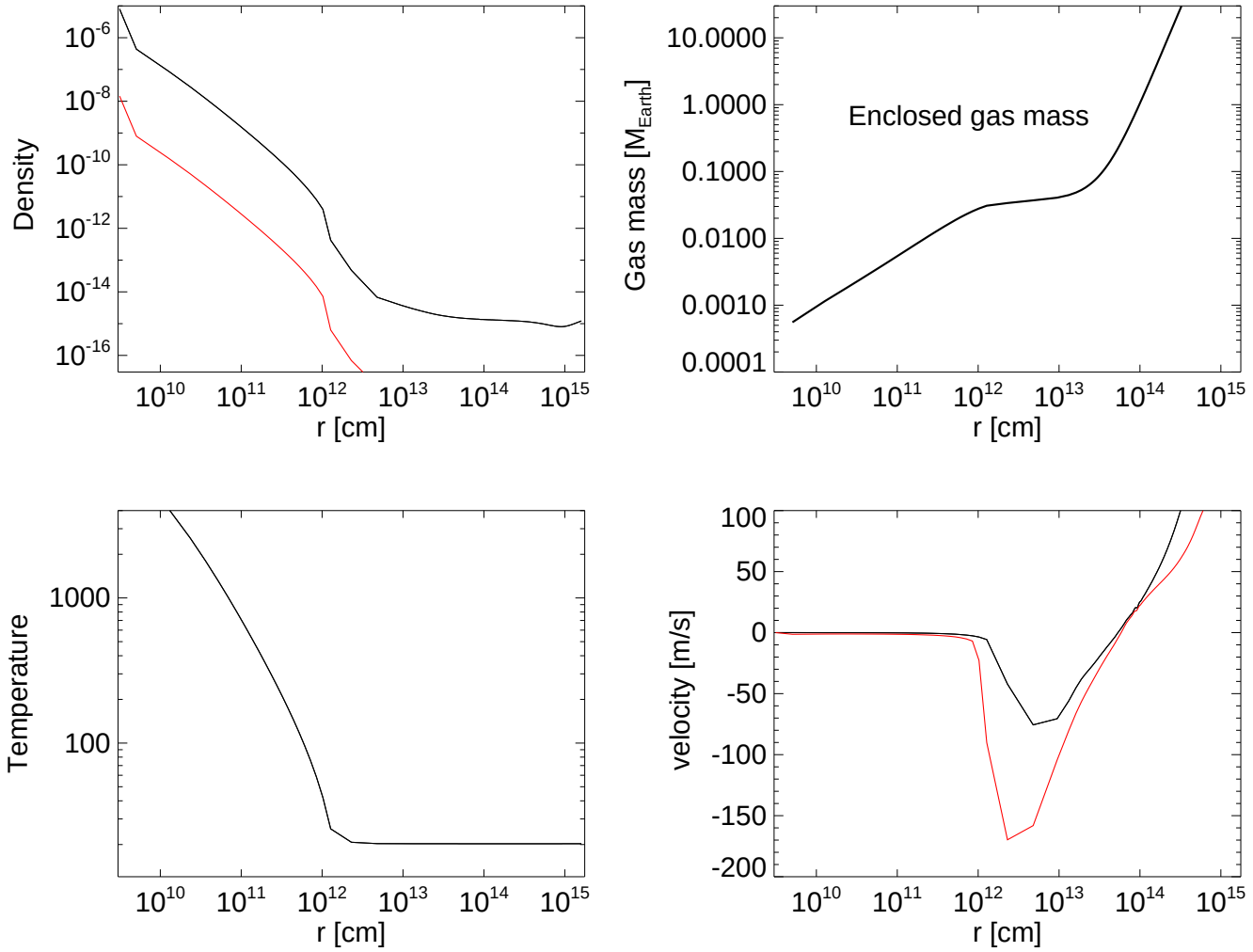

Figure 7. The radial structure of the first core near the end of simulation M0α3, at time $t = 3.16 \times 10^4$ yrs. The upper right panel shows the enclosed gas mass in Earth's masses.

positive rather than the usual negative gradient in the ratio of ρ_d/ρ, e.g., a relative deficit of grains in the centre of the first core. Turbulent diffusion mixing then reverses its effects and actually increases the grain accretion rate near the core while of course continuing to impede grain sedimentation at larger radii.

5 DEPENDENCE OF RESULTS ON THE MASS OF THE FIRST CORES

Having studied grain sedimentation and high-Z core building for $M_{\rm fc} = 10M_J$ in some detail, we shall now review the results of the less and more massive runs shown in Table 1.

5.1 "Heavy" first cores

The most massive first core case studied in the paper is $M_{\rm fc} = 20M_J$, shown in Table 1 with IDs starting with letter "H". Only one value of turbulent parameter is considered for these simulations, $\alpha_d = 0.001$. It is immediately obvious that these most massive cores are the least promising sites of grain sedimentation, which is also in accord with the results of paper I. Only the high opacity cases, $\kappa_0 = 0.1$ and 1, resulted in significant high-Z cores. The physical reason for this is their already hot initial state. These cores rapidly evaporate their grains, if allowed to cool at a reasonably rapid rate.

The inefficiency of the process of dust sedimentation for these most massive cores stands out clearly. The most massive solid core assembled, $M_{\rm core} = 12.2\,{\rm M}_\oplus$, represents only about a quarter of the condensible high-Z mass available inside the gas clump for $M_{\rm fc} = 20M_J$.

5.2 "Low mass" first cores

Finally we come to the lightest first core case we studied in this paper, $M_{\rm fc} = 5M_J$. Concentrating on the first four entries starting with letter "L" in IDs in Table 1, one notices that these runs all produce high-Z cores with masses above $1\,{\rm M}_\oplus$. The efficiency with which the grains are locked into the central core reaches 100% in L0α3 and L1α3.

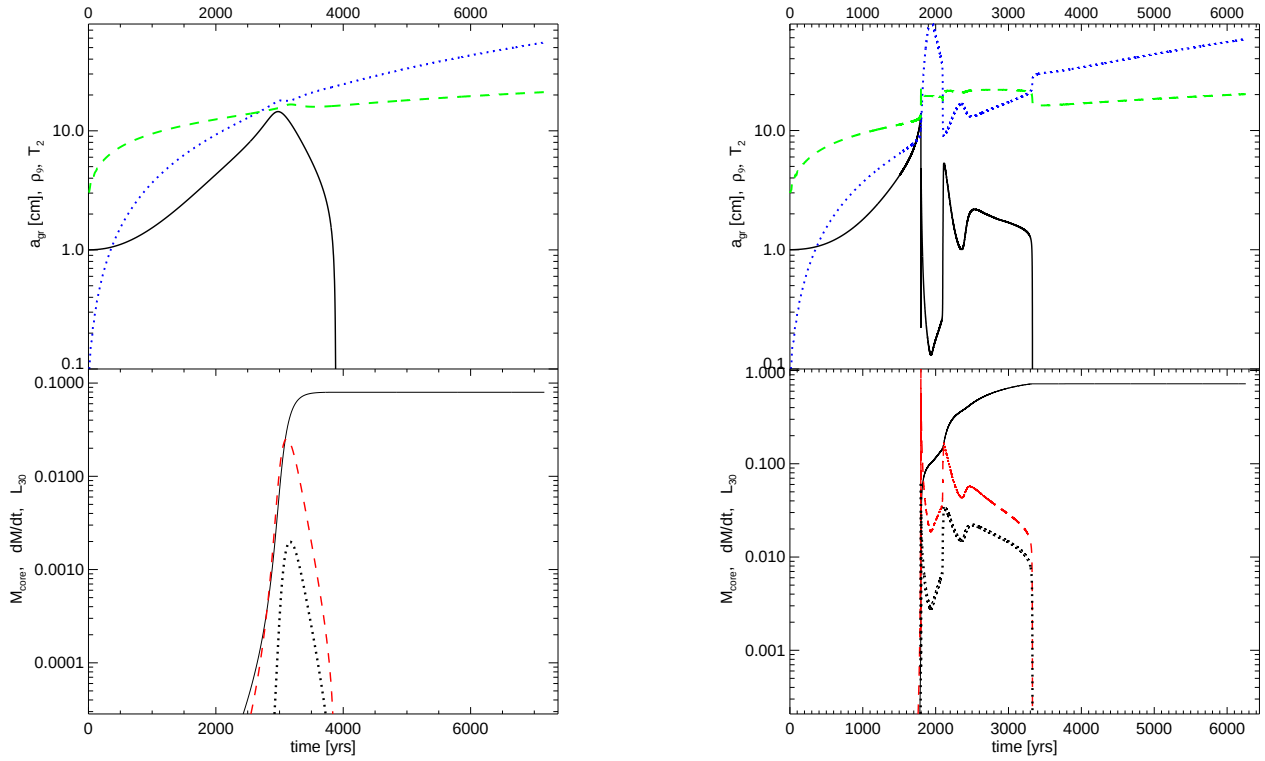

Figure 8. Same as figure 1 but for simulation M2α2 (Left panel) and M2α4 (Right panel). Note that in both simulations the end mass of the solid core is lower than that in A2α3, but for different reasons. See text (§4.5) for a further explanation.

Looking at further entries in the Table, we find the familiar trends with the turbulent mixing parameter α_d: higher values of it usually result in smaller values for $M_{\rm core}$. The turbulence needs to be rather extreme to prevent the formation of high-Z cores completely: a very high turbulence run, $\alpha_d = 0.1$ (L0α1), resulted in a core of $0.075\,{\rm M}_\oplus$ mass, albeit after a very long ($\sim 10^5$ years) time.

The physical reason for the resilience of dust sedimentation process in lower mass cores is that the initial temperature in such is low, e.g, $\lesssim 100$ K (see the lower panel of Figure 1 in paper I). Both cooling and vaporisation times in the low mass first cores are long, and hence dust has a plenty of time to grow and sediment, even in the presence of turbulence.

6 LONG TERM EVOLUTION

6.1 Expectations: Giant planets with solid cores?

The solid core – gas envelope structure we study here is essentially the same as that studied by many authors in the context of the core accretion model for giant planet formation (e.g., Pollack et al. 1996). The difference is mainly in the environmental factors by which we mean boundary conditions "far" from the solid core. Furthermore, the solid cores that we study here also grow by accretion of solids. We should thus expect that at least some of the classical core accretion model results may pertain to the problem we study.

One such result concerns the build up of a massive gaseous atmosphere around the solid core. For low solid core masses, the atmosphere is in a hydrostatic equilibrium, in which the gravitational force due to the solid core and the gas own weight is balanced by the pressure gradient. As shown by Mizuno (1980), when the solid core mass increases and exceeds a critical value, $M_{\rm crit}$, a hydrodynamical collapse driven by self-gravity of the gas takes place. The gaseous envelope contracts to much higher densities. This marks transition from a hydrostatic balanced atmosphere to a gas accretion phase. The latter goes on as long as there is gaseous fuel supplied from outside. Adding accretion of solids from the protostellar disc one arrives to a very crude sketch of the core accretion model (e.g., Pollack et al. 1996).

There is a scope for a conceptual confusion here. The giant planet embryo is itself a massive gaseous self-gravitating "atmosphere" around the solid core. But the bulk of this gas is not bound to the solid core at all as the mass of the latter is rather small. Initially, the gas pressure gradient is nearly zero in the central part of the gas cloud since weight of the central region is small (proportionally to $\sim R^3$). It is the weight of the layers above that keep the innermost gas from expanding outward. Appearance of a solid core in this constant pressure, constant density, environment, at first has little effect as the gas pressure is too high. However, as the mass of the solid core increases, there is a critical point as

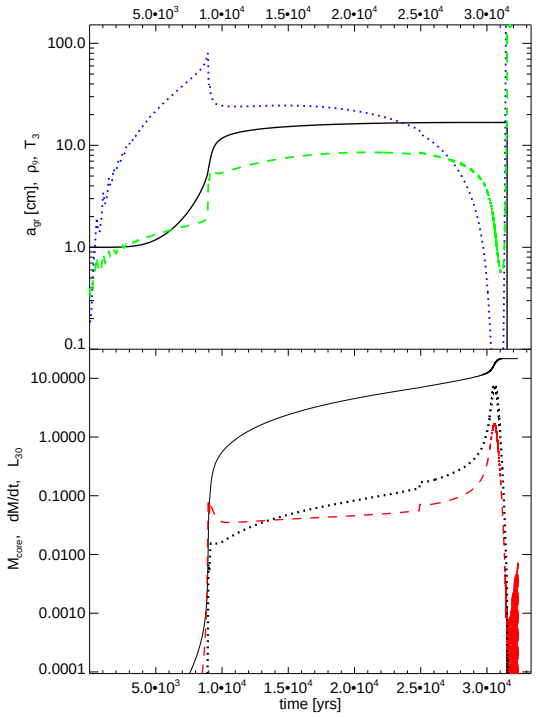

Figure 5. Same as figure 1 but for simulation M0α3. In constraint to that figure, however, the density is plotted in units of 10^{-12} g cm^{-3}. Note the trough and then a spike in the temperature and density values near the end of the simulation. This marks building of a dense and hot atmosphere around the solid core (cf. figure 6).

in the calculation of Mizuno (1980) at which the gas around the solid core starts to collapse on it and forms an atmosphere around it. This "atmosphere within and atmosphere" is gravitationally bound to the solid core and itself. It is much denser and becomes distinct from the giant embryo. In paper III we argue that when the embryo is disrupted by tidal forces of the parent star, the inner solid-core bound atmosphere may survive. The result is probably not unlike a giant planet built in the core accretion model, although detailed calculations beyond the scope of our paper are needed to characterise its chemical composition and other properties. Nevertheless, one robust prediction is a metal rich composition of a giant planet built inside a more massive giant embryo gas clump: the abundance of dust in the central regions of the embryo is enhanced by dust sedimentation.

6.2 Numerical issues

The most straightforward way to explore these ideas would be to study them numerically. In the simulations listed in Table 1, there is only one example of a bound gas atmosphere, the simulation M0α3, and even then the atmosphere weighs only $0.03\,\mathrm{M}_\oplus$, which is about 0.001 of the mass of the high-Z core for that simulation.

We suspect that at least the more massive of the solid cores built up in our simulations should be surrounded by massive gaseous atmospheres at later times. Computational limitations of our method precluded us from studying this interesting question in detail.

As explained in §3.1, we need a hydrodynamics rather than hydrostatics based approach to follow the evolution of the system during the phases of a rapid gravitational collapse or the bounces driven by too much accretion onto the solid core. Unfortunately this hydrodynamical approach also makes it difficult to evolve the system for long periods of time after the formation of the solid core if the core starts to build up a massive gaseous atmosphere. As an atmosphere starts to build up around the solid core, time steps become very short, and the code basically stalls.

Being unable to follow the evolution of the system into the appropriate regime numerically, we resort to analytical arguments and analogies to the classical core accretion model results.

6.3 Minimum critical (cold) solid core mass

The temperature profile of the gas is the main uncertainty in our calculation here. The lower the gas temperature, the smaller is the gas pressure gradient for a fixed density profile. Therefore, by choosing appropriately a minimum possible temperature that the gas near the solid core may have we should be able to obtain the minimum required solid core mass for atmosphere collapse.

A simple way of doing this is to consider a giant embryo unperturbed by the energy release from the solid core, setting $L_{\rm acc} = 0$. This is satisfied by those of our models that had grains evaporated after the core assembly (e.g., see the right panel of figure 8). Further, somewhat unrealistically, we shall assume that the gas remains isothermal even in the presence of the solid core's potential. The result is nevertheless interesting as a lower limit to the mass of the solid core at which a massive gaseous atmosphere can be built.

With these ideas in mind, our treatment here echos that presented in section 6.1 of Armitage (2010) (note that the derivation was first made by Sasaki 1989). The hydrostatic balance equation for isothermal gas surrounding the solid core is

$$c_s^2 \frac{d\rho}{dR} = -\frac{GM_{\rm core}}{R^2} - \frac{GM_e(R)}{R^2}\ , \qquad (13)$$

where c_s is the isothermal sound speed, $M_e(R) = \int_{R_{\rm core}}^{R} 4\pi r^2 \rho(r) dr$ is the enclosed gaseous envelope mass inside radius R, and $R_{\rm core}$ is the radius of the solid core. If a hydrostatic balance solution exists, then the density given by equation 13 should smoothly join the unperturbed first core density at radii R where the gravity of the solid core is negligible.

We first consider the case when the gaseous envelope is much less massive than the core, and thus we neglect the last term in equation 13. The solution is then trivial:

$$\rho(R) = \rho_{\rm fc} \exp\left[\frac{GM_{\rm core}}{Rc_s^2}\right] \quad \text{for} \quad R > R_{\rm core}\ . \qquad (14)$$

Note that $\rho(R) \to \rho_{\rm fc}$ at $R \to \infty$, as needed.

The factor in the exponential can be very large near the solid core. In that case it also drops off very quickly with the distance from the first core. Hence, the mass of the atmosphere around the solid core is approximately

$$M_{\rm atm} \sim \frac{4\pi}{3}\rho_{\rm fc} R_{\rm core}^3 \exp\left[\frac{GM_{\rm core}}{R_{\rm core}c_s^2}\right] \ . \quad (15)$$

This treatment is valid as long as $M_{\rm atm} \ll M_{\rm core}$, since in the opposite case the weight of the atmosphere cannot be neglected in equation 13, as we have done above. Self-gravity of the gas around the solid core initiates a "collapse" of the gaseous atmosphere. The critical mass of the solid core when the collapse happens is found by setting $M_{\rm atm} = M_{\rm core}$. We call the corresponding core's mass a "critical cold" mass:

$$\frac{GM_{\rm cold}}{R_{\rm core}c_s^2} \approx \ln\left(\frac{\rho_c}{\rho_{\rm fc}}\right) = 20\Lambda \ , \quad (16)$$

where $\Lambda \equiv \ln(\rho_c/\rho_{\rm fc})/20 \approx 1$ for $\rho_{\rm fc} \sim 10^{-11}$ g cm^{-3}. As the first core density enters logarithmically, the result is weakly dependent on the value of Λ. Eliminating $R_{\rm core} = (3M_{\rm core}/4\pi\rho_c)^{1/3}$, we have

$$M_{\rm cold} = \left(\frac{3}{4\pi\rho_c}\right)^{1/2} \left(\frac{kT}{\mu G}\right)^{3/2} \ln^{3/2}\left(\frac{\rho_c}{\rho_{\rm fc}}\right) \quad (17)$$

This expression is similar to that for Jean's mass, but with the density of the solid core rather than the gas density inserted, and the logarithmic factor Λ. Numerically,

$$M_{\rm cold} = 2.7\ {\rm M}_\oplus\ \frac{T_3^{3/2}}{\rho_p^{1/2}} \left(\frac{2.45}{\mu}\right)^{3/2} \Lambda^{3/2} \ . \quad (18)$$

This estimate is robust in the sense that the temperature of the unperturbed first cores does not vary all that much. As found in paper I, by the time grains sediment to the centre the temperature of the gas is typically between a few hundred K and 1400 K. The upper value for the temperature range is set by vaporisation of grains, whereas the lower one is simply due to a rapid cooling of first cores: as we found in paper I, the first cores cool initially very rapidly since they are spatially extended and only mildly optically thick.

A correction downward to the minimum critical core mass is needed in the case when the density of the dust around the solid core is comparable or higher than that of the gas. One should then adjust the mean molecular weight in equation 18 to reflect the metal-rich composition of material in the inner region of the first core.

6.4 Maximum critical (radiative) core mass

The isothermal envelope assumption that we used above allowed us to explore one extreme of the problem at hand, e.g., when the envelope temperature is completely unaffected by the presence of the solid core. An opposite extreme assumption is that the immediate envelope around the solid core is much hotter and denser than the giant embryo in which it is embedded, so that the presence of the latter is a minor detail. This may nearly be the case if the luminosity of the solid core is very high, e.g., comparable with the total cooling luminosity of the giant embryo. This set of assumptions constitutes the "radiative zero" solution to the gaseous atmosphere structure (Stevenson 1982).

The radiative zero solution also makes a prediction for the critical solid core mass (see below), which we shall call $M_{\rm rad}$. In contrast to the "critical cold" mass derived above, $M_{\rm rad}$ is likely to overestimate the critical core mass. The radiative zero solution assumes zero pressure and density boundary conditions at infinity. In contrast, our envelope is surrounded by material of a relatively high density and pressure. At large distances from the solid core, gas density and temperature should join the values of these quantities in the first core, rather than go to zero. The additional pressure and weight of the outer cooler envelope of the giant embryo is certain to lower the critical mass of the solid core required to initiate the collapse.

The central quantity in the radiate zero solution is the luminosity of the solid core, which is derived from accretion of planetesimals. We thus need to estimate the typical accretion rate onto the core. The sedimentation time scale of grain material, $t_{\rm sed}$ has been estimated in paper I, and is usually between 10^3 to a few $\times 10^4$ years. Assuming that $M_{\rm Z,c} \sim 20\,{\rm M}_\oplus$, and that all this solid core-building material falls onto the core within 10^4 years, we find the solid core accretion rate, $\dot{M}_{\rm core}$, is

$$\dot{M}_{\rm core} \sim 2\times 10^{-3}\,{\rm M}_\oplus\ {\rm yr}^{-1} \ . \quad (19)$$

Ikoma et al. 2000 updated and expanded the results of Stevenson (1982) for a broad range of opacities in the envelope (which were assumed temperature independent in contrast to our power-law dependence). In particular, they provided a power-law fitting formula to the critical core mass. Using that formula for a fiducial opacity coefficient value of $k_{\rm gr} = 0.01$, we have

$$M_{\rm rad} \sim 25\ {\rm M}_\oplus \left(\frac{\dot{M}_{\rm core}}{2\times 10^{-3}\,{\rm M}_\oplus{\rm yr}^{-1}}\right)^{q'} \left(\frac{k_{\rm gr}}{0.01{\rm cm}^2{\rm g}^{-1}}\right)^{s'} \quad (20)$$

where $q' \approx s' \approx 1/4$.

6.5 Summary on critical core mass and further complications

We have argued above that there should be a critical solid core mass, $M_{\rm crit}$, above which the initially tenuous gas atmosphere around the core is unstable to self-gravity and should collapse. The collapse should build a *massive* gas atmosphere atop the solid core. The composition of the atmosphere should be metal rich as the interior of the giant embryo is metal rich due to dust sedimentation. This object inside the giant embryo may have properties similar to giant gas and giant icy planets (as pointed out by Boss et al. 2002).

As far as the value of $M_{\rm crit}$, we suggested that it is limited from the bottom by $M_{\rm cold}$ and from the top by $M_{\rm rad}$. For typical parameters the range here is from a few to few tens of Earth masses.

However, for the most massive embryos, say $M_{\rm fc} \gtrsim 200$ Jupiter masses, it is possible to get the gas to collapse gravitationally and form a compact proto-planet without a solid core at all (see below), especially if dust opacity can be made very small. In this case the embryo may reach vaporisation temperature before dust sediments.

Our numerical code assumes that hydrogen is molecular, which is a very reasonable assumption for the first cores before they undergo the second collapse (Masunaga et al. 1998; Masunaga & Inutsuka 2000). This assumption may be violated when a dense and hot gas atmosphere builds up around the core, or when the whole first core contracts sufficiently to surpass $T \approx 2000$ K. As with collapse of first

cores, hydrogen molecules disassociation and then hydrogen atom ionisation energy losses at even higher temperature may help gravitational collapse of the atmosphere.

Therefore, *if the first core is truly isolated* and is allowed to contract in peace (rather than being tidally or irradiationally disrupted after a finite amount of time, paper III), then the whole first core can eventually collapse onto the solid core. This "second" wave of collapse is completely analogous to that of the first cores in star formation (Larson 1969), and is not at all initiated by the solid core. Hence *truly isolated* giant planet embryos could presumably contract into giant planets with arbitrary small solid cores, including none.

7 ON ASSEMBLY PROCESS OF TERRESTRIAL PLANET CORES

In §6 we proposed that giant planets with solid cores may form inside the giant embryos when the solid cores grow more massive than the critical mass, $M_{\rm cr}$. We further argued that this part of the planet formation picture may be quite similar to that worked out in the classical core accretion schemes, albeit for different accretion rates of solid material and boundary conditions "far" from the solid core.

In contrast, the earliest stages of the solid core assembly could not be more different. We believe it is far "easier" to form massive solid cores inside the giant embryos at large distances from the star than it is in situ at $R \sim$ few AU in the "standard" bottom-up build-up scenario (e.g., Safronov 1969; Wetherill 1990). The numerical treatment of dust sedimentation inside the first cores (= giant planet embryos) that we employed in this paper may have obscured this important point, which we shall discuss below in detail.

7.1 The standard bottom-up scenario: the key role of planetesimals

The core accretion model – (e.g., Safronov 1969; Mizuno 1980; Wetherill 1990; Ida & Lin 2008), also reviewed in chapters 4-6 in Armitage (2010) – stipulates that planet formation starts on smallest scales, with dust initially growing inside the protoplanetary disc into larger grains. This very first part of the picture is physically similar to the model of Boss (1998) and what we assumed here, with dust growing by gentle hit-and-stick collisions (Blum & Wurm 2008). There is then a poorly understood step of building planetesimals, which are solid bodies of $\gtrsim$ km size. Once planetesimals are assembled, "planetary embryos" – 10^3 km sized bodies are built by collisions of planetesimals, and finally Earth mass terrestrial cores are accreted by giant impacts of such embryos (Safronov 1969).

Due to well known problems with planetesimal assembly authors used to urge a leap of faith, arguing that if planetesimals had not been assembled somehow, we would not be here, and that "Nature knew how to do it" (e.g., Wetherill 1990). This is clearly unsatisfactory. Most solid matter outside the Sun in the Solar System is inside the cores of the giant planets and also in the terrestrial planets. Thus the total mass of planetesimals must have been at least equal to the total mass of the solids in the Minimum Mass Solar Nebula (MMSN, Weidenschilling 1977b), and hence most of the solids in the disc (= "nebula") must have been reprocessed through planetesimals.

Recent conceptual breakthroughs suggest that solids may be concentrated into larger structures by instabilities and turbulence in the disc (e.g., Youdin & Goodman 2005; Johansen et al. 2007; Cuzzi et al. 2008), although it is too early to say that the planetesimal step assembly is understood. Studies of collisional evolution of asteroid-like bodies suggest that the initial size of planetesimals must be larger than the classical $\sim few$ km size objects, and be in the 100 to 1000 km size range (e.g., Morbidelli et al. 2009), thus increasing the requirements for the planetesimal buildup models.

In any event, we shall now review the well known reasons why terrestrial planet cores cannot be built in the CA model directly, and argue that these difficulties are avoided if massive solid cores are made inside giant planet embryos.

7.2 Kepler shear: limiting the mass of fragments

The most direct route to "large" solid objects in the CA model is the gravitational instability of a dense dust layer (Safronov 1969; Goldreich & Ward 1973). It works best if there is no turbulence in the gas, as turbulence provides support against gravitational collapse. We hence first assume that turbulence is absent. Inside a protostellar disc, Kepler shear limits the maximum mass of the clump of solid material that can collapse into one body to (e.g., §4.6.2 in Armitage 2010)

$$m_{\rm fr} \sim 4\pi^5 \Sigma_{\rm sol}^3 G^2 \Omega_K^{-4} \ , \qquad (21)$$

where $\Sigma_{\rm sol}$ is the column density of solid material in the disc, and Ω is the Keplerian angular frequency at that location. At 1 AU, $\Sigma_{\rm sol} \sim 10$ g cm^{-2} (Weidenschilling 1977b) . Thus, at the location of the Earth this yields $m_{\rm fr} \lesssim 10^{-9}$ Earth masses.

This shows that even in the most optimistic scenario one must start with very small bodies and continue by building up larger bodies in collisions (e.g., Morbidelli et al. 2009). The origin of the problem here is in the differential shear of the disc that limits the largest possible wavelength of gravitational instability (e.g., Toomre 1964) to only $\sim 10^8$ cm (see §7.3 below).

Now, the mass of the solids inside of a bound fragment in the gravitationally fragmenting *gas* disc is much larger, e.g.,

$$m_{\rm fr} \sim f_g M_* \left(\frac{H}{R}\right)^3 \ , \qquad (22)$$

which for $H/R \sim 0.1$ yields at least a few Earth masses. This is because (a) the parent gravitationally collapsing body is a gas disc, not a dust one, and (b), the Keplerian shear at 100 AU is 10^3 times weaker than it is at 1 AU.

7.3 Kepler shear and turbulence: preventing collapse

Kepler shear has another undesirable effect on the potential gravitational collapse of solid material inside the protoplanetary disc. To become gravitationally unstable, the density of the layer must exceed the tidal density, which is of the order of 10^{-7} g cm^{-3} at 1 AU. Thus the thickness of the

layer must be less than $H_{\rm max} = \Sigma_{\rm sol}/\rho_{\rm t} \sim 10^8$ cm. In equilibrium, the thickness of the layer of solid particles depends on their random, e.g., turbulent, velocities. These must be less than $v_t \lesssim (H_{\rm max}/R)v_K \sim 10^{-5}v_k = 30$ cm s^{-1}. This is extremely small compared with the expected sound speed of $\sim$ km s^{-1}. Such small turbulent velocities appear very unlikely given the instabilities in the turbulent Ekman boundary layer (Weidenschilling 1980) excited by the differential rotation of solids and the gas. Thus building up solid bodies as small as 10^{-9} M$_\oplus$ by gravitational collapse in the CA model is not straightforward.

Now contrast this picture to the gravitational collapse of the dust sphere settling inside the first core, a process analogous to the dust layer gravitational collapse. As shown in paper I, gas pressure effects become negligible when the grain sphere contracts to the "grain cluster" density $\rho_{\rm gc} = \rho_{\rm fc} f_g^{-1/2}$. Self-gravity of the grain cluster at this point exceeds gas pressure gradients. The radial size of the grain cluster is $R_{\rm gc} = R_{\rm fc} f_g^{1/2}$, which is typically about $0.1AU$, and the mass is $f_g M_{\rm fc}$. The turbulent velocity required to keep the grain sphere from collapse is

$$v_{\rm t,min} \sim \left(\frac{G f_g M_{\rm fc}}{R_{\rm gc}}\right)^{1/2} \approx f_g^{1/4} c_s \ , \qquad (23)$$

where $c_s = \sqrt{kT/\mu} \approx \sqrt{GM_{\rm fc}/R_{\rm fc}}$ is the sound speed of the first core. As temperature of the first core is of order 10^3 K, we find

$$v_{\rm t,min} \sim 0.6 \text{ km s}^{-1} \left(\frac{f_g}{0.01}\right)^{1/4} T_3^{1/2} \ , \qquad (24)$$

This velocity is roughly 30% of the gas sound speed in the first core, and is about 2000 times higher than the minimum turbulent velocity found for the dust layer in the CA model. It seems very doubtful that the first core would support such a strong turbulence. In contrast to the differentially rotating Keplerian disc, the first core may be expected to be in a solid body rotation with angular frequency characteristic of the disc at $R_p \sim 100$AU, e.g., 3 orders of magnitude slower than at 1 AU.

These estimates are supported by our numerical results: even the highest turbulent parameter run, $\alpha_d = 0.1$ (L0α1), yielded a rather massive solid core (cf. Table 1).

7.4 Collisional buildup of planetesimals in CA model

As the direct gravitational collapse to form (even such small bodies as) planetesimals is complicated by turbulence in the CA model, alternative ideas to form them via non-gravitational growth mechanisms have been thoroughly explored (e.g., Dominik & Tielens 1997); for a recent review see Blum & Wurm (2008). One could hope that the solids in the disc continue to grow via collisional agglomeration as smaller dust is believed to do. However, there are two principal problems with this hit-and-stick idea also. Firstly, due to drag from the gas, the grains of different sizes are calculated to move at different speeds; $\sim$ metre size objects should be colliding at velocities of $\sim$ ten metres per second (Weidenschilling 1977a). Common sense and lab experiments (Blum & Wurm 2008) suggest that growth, i.e., sticking of the collisions partners, is rather unlikely at these high speeds. The second problem is frequently referred to as the *metre-size barrier*. In a non-turbulent protoplanetary disc, the $\sim$ metre size objects must spiral radially inward, into the parent star, on time scales of order a few hundred years, well before they could grow to larger sizes (Weidenschilling 1977a).

7.5 Planetesimals are not needed to build terrestrial planet cores inside giant embryos

We find that neither the problem with too-energetic collisions for the hit-and-stick growth nor the radial drift problem appear to exist if solid bodies grew inside the protective environment of the giant embryo. The radial drift problem is most obviously absent: solids migrate with the embryo rather than individually.

Furthermore, we shall now show that solids that contribute the most to the terrestrial planet cores inside the giant embryos are not planetesimals, and not even boulders, but are meager pebbles. The collisions of such small bodies are gentle. This resolved the issue with too fast collisions that tend to fragment dust aggregates rather than bind collision partners together in the CA model.

As we found in paper I, while grains are microscopic, turbulence keeps them from sedimenting down very efficiently. The equilibrium reached between sedimentation and turbulent mixing with the turbulent diffusion coefficient α_d sets the radial scale of the dust distribution $H_d \sim R_{\rm fc}(\alpha_d \rho_{\rm fc} R_{\rm fc} \lambda/\rho_a a^2)^{1/2}$ (see paper I). We picked the "large" grain size limit here, when $a \gg \lambda \approx 4$ cm $(10^{-9}/\rho_{\rm fc})$, the mean free path in the gas. Requiring now that the equilibrium scale-height H_d be smaller than the grain cluster size $R_{\rm gc}$ – at which point the grain cluster could collapse due to self-gravity – we infer that grains must be larger than

$$a_{\rm min} \sim 80 \text{ cm } \left(\alpha_{-3} f_{-2}^{-1} \rho_a^{-1} \frac{R_{\rm fc}}{1\text{AU}}\right)^{1/2} \ , \qquad (25)$$

where $\alpha_{-3} = \alpha_d/10^{-3}$.

The estimate above predicts that the grains should grow to about 1 m size in order for gravitational instability to overwhelm turbulent mixing. However, we must keep in mind that the estimate is based on a number of approximations; e.g., estimating the properties of the "grain cluster" based on the maximum gas pressure gradient possible (paper I). Numerical experiments in the present paper have shown that the "runaway phase" of core accretion, which occurs when the grain cluster starts to collapse, takes place when the grains reach dimensions of 10-20 cm (cf. figures in this paper), rather than 80 cm.

We can now estimate the sedimentation velocity of grains of this characteristic size:

$$u_{\rm sed} = \frac{4\pi G \Sigma_a R_{\rm gc}}{3 c_s} \frac{a}{\lambda} \ . \qquad (26)$$

Since $R_{\rm fc}/c_s \approx 1/\sqrt{G\rho_{\rm fc}}$, we can rewrite this as a function of the gas density of the first core at the moment of the grain cluster formation:

$$u_{\rm sed} \approx 0.7 \text{ m s}^{-1} \left(\frac{a}{10\text{cm}}\right)^2 \rho_a f_{-2}^{1/2} \rho_{-9}^{1/2} \qquad (27)$$

This estimate is consistent with our numerical results – the grain sedimentation velocity is below 10 m/s in the innermost part of the first core identifiable as the "grain cluster".

One caveat here is that we have so far assumed a non-rotating giant embryo. However, comparing the stopping time of a grain defined as $u_a/|du_a/dt|$, one finds that only grains larger than 10^3 cm or more would be in the "perturbed Kepler orbit" regime (Weidenschilling 1977a) in which the particle moves essentially on its Keplerian orbit experiencing little drag from the gas. The particle's angular momentum suspends it some distance away from the cloud centre, and it spirals in slowly due to gas drag forces. This implies that small particles dominating the grain sedimentation process are in the opposite regime, e.g., approximately following the rotation of the gas. As long as the embryo is not completely supported by rotation, the local rotation speed is lower than the circular orbit value. Thus small grains cannot be supported by rotation against gravitational collapse, and our spherically symmetric treatment should be reasonably representative of slowly rotating giant embryos.

Having said this, we note a sort of reincarnation of the "metre-size barrier" problem for dust in rotating giant planet embryos – even larger than 1 metre dust grains are going to be lost into the centre of the embryo – but that is not a problem at all. The grains sinking into the centre of the cloud are not lost into the star but presumably join the solid core there, therefore they are not "lost" in any sense.

7.6 Summary on direct gravitational collapse

Summarising these points, it appears that a direct build up of massive terrestrial-like cores is possible inside the first cores (giant planet embryos) due to a favourable (spherical) geometry and low shear. One interesting point of the present picture is that the building blocks of the solid cores of terrestrial planets are grains of ~ 10 cm size rather than planetesimals of km or more size. While numerical 3D simulations, well beyond the scope of our paper, are needed to model the amount of mass put into bodies of different sizes, there is no clear theoretical need to put much mass into the planetesimal population inside the embryo at any time. This is in contrast to the core accretion model where terrestrial planets are made of planetesimals. We hence expect (pending future confirmation by numerical simulations) that the relative amount of mass in asteroids and comet-like bodies compared to that in terrestrial cores is much smaller in our model than traditionally assumed.

Finally, there is no loss of solids problem as in the disc geometry – any solids lost into the centre of the giant embryo actually contribute to the growth of the solid core there.

8 DISCUSSION

8.1 Summary of numerical results

We have argued that clumps formed by the GI in protoplanetary discs at $R \sim 100$ AU should be similar to that of the first cores (Larson 1969). Using a two-fluid radiative hydrodynamics code, we found that the dust inside the gas clumps may grow and settle into a core if the gas remains cooler than the grain vaporisation temperature. The high-Z elements core may become massive ($\sim 10\,\mathrm{M}_\oplus$) if feedback processes are not too severe. Our results are more restrictive than analytical estimates of Boss (1998); Boss et al. (2002). On the other hand, the maximum masses of the solid cores that we find are larger than those of Helled et al. (2008); Helled & Schubert (2008).

As already indicated in the Introduction, the main difference with the latter authors appears different initial conditions for the gaseous clumps. For example, all of the $M > 5M_J$ mass clumps in Table 1 of Helled & Schubert (2008) are unable to form any solid cores because they are already hotter than $T = 1400$ K at birth. In contrast, the initial temperature of a $M_{\rm fc} = 5M_J$ clump in our model is only about 60 K (cf. equation 4). These clumps do cool initially very rapidly, increasing in temperature to hundreds of K, but their increased density allows for an accelerated grain growth too (see fig. 1-3 in paper I). We also found that our initial conditions are stable to convection, and thus convective grain mixing does not significantly impede grain sedimentation. Convection becomes important once a massive and radiatively bright solid core forms, but by that time grains may be large and the central region dominated (by density) by the grains, thus the effects of convection remain subdued compared with the results of Helled et al. (2008); Helled & Schubert (2008).

8.2 Astrophysical implications

We discuss observational implications of these results in a follow-up paper (paper III) where we take into account additional processes not discussed here: radial migration of the giant planet embryos and their Tidal and Irradiative Evaporation (TIE) when the embryos come too close to the parent star. Therefore here we only briefly mention the implications directly following from the results presented here and in paper I.

We believe that grain sedimentation inside the giant planet embryos at tens to a few hundred AU distances from the parent star is a viable process by which to form terrestrial mass solid cores. We argued in §7 that a direct gravitational collapse of ~ 10 cm-sized solids in the central region of the gas clump can make massive solid cores directly without the need to go through objects of intermediate sizes (such as planetesimals and Moon-sized objects). Neither turbulence nor the high speed collisions (absent in TIE in the stages before the grain cluster collapse) appear to be serious obstacles to the gravitational collapse of the solid component.

We also argued that massive gaseous atmospheres around the solid cores should start building up once the latter reach a critical mass which is in the range of a few to a few tens Earth masses. The arguments here are similar to the classical core accretion picture for building the giant planets (Mizuno 1980; Pollack et al. 1996) except that the gas is accreted not from the disc but from the surrounding gaseous envelope of the first core. This potentially can make a metal rich (as the interior of the first core is such) giant planet with a solid core. Removal of the outer metal poor gaseous envelope, discussed in the follow-up paper, could then produce classical giant planets such as Jupiter.

In addition to the tidal disruption and irradiative evaporation of the envelope by the parent star, gaseous clumps may self-unbind themselves due to an excessive heat release by the solid cores within them if envelope opacity is high. These effects may be even more important for rotating first cores (rotation is expected for first cores formed

in a disc, e.g., Levin 2007). Indeed, the amount of energy needed to unbind the core is then reduced. Furthermore, following the suggestion of Boss et al. (2002), the gaseous envelope of the first cores may be removed by a strong ionising radiation of a passing OB star. This is clearly more realistic for first cores as these are initially very fluffy objects (see also Whitworth & Zinnecker 2004), but more work is needed here. We plan to address the issue in our future work.

The processes discussed here may create terrestrial mass solid planets at large distances from the parent star. In addition, the escape velocity form first cores is less than a few km s^{-1}. Collisions of such rotating clumps with each other may perhaps unbind a fraction of the solid material there, contributing to the population of solids at these large radii (see also Clarke & Lodato 2009).

Finally, we note that the proposed route to formation of terrestrial and giant planets is somewhat a of a hybrid between the two current competing models, e.g., the gravitational instability and the core accretion models. In TIE the planet formation process begins with gravitational instability (gas clump formation, grain sedimentation and core growth) but continues with as in core accretion (accretion of gas onto the solid core).

8.3 Shortcomings of the calculations

Despite using a relatively sophisticated two-fluid radiation hydrodynamics approach, our treatment here is still quite far from being sufficient. In particular, hydrogen molecules dissociation and hydrogen ionisation should be taken into account in the future to allow higher resolution studies of the innermost region near the solid core. Introducing several different species of grains with different vaporisation temperature is desirable, as is allowing the grain size to vary from bin to bin, instead of assuming one size as we have done here. Turbulent and convective mixing for grains may be improved. Furthermore, we have neglected effects of rotation of the first core here. Finally, the dust opacity, independent and fixed in our calculation, should of course evolve as dust grows and sediments, but it is hard to see how a self-consistent and yet not overly complicated treatment of these effects could be done at the present.

We expect these effects to modify the results of our dust sedimentation calculations. Nevertheless, we feel that our exploratory calculations are interesting in showing the possible range of behaviour in the given problem.

8.4 Connection to previous ideas and work

As spelled out in the Introduction, our work is an extention and an update of the Boss (1998); Boss et al. (2002) ideas. We find that giant planet embryos born at $R \sim 100$ AU should be similar in their initial properties to the first cores. These cooler and fluffier gas configurations present a perfect birthplace for massive solid cores. In paper III we argue that giant planet embryos migrate inward and get tidally disrupted there. This hypothesis is similar to the ideas of Boss and co-authors, although the exact protoplanetary disc setting is different.

There is also some similarity between our ideas and that of Rice et al. (2004); Clarke & Lodato (2009), who have recently argued that some fraction of planetesimals may form inside gas pressure maxima provided by spiral arms in self-gravitating protoplanetary discs at $R \gtrsim 30$ AU. These spiral arms are stable for about a rotation, during which time the density enhancement in the arms, compared to the mean density in the disc, may be significant if the cooling time in the disc is short enough. The location of the marginally stable *non-fragmenting* region of the disc is somewhat inside the fragmenting region that we discuss (see Fig. 1 in Clarke & Lodato 2009). Our study is thus an extension of these ideas on the larger disc scales, where spiral arms do fragment, and where the density enhancement is much greater than unity.

Furthermore, we note that, having submitted papers I and III, and having almost finished the final draft of the present paper we discovered a set of even more closely related ideas on formation of terrestrial planet cores inside giant planet embryos in a recent paper by Boley et al. (2010). In addition, Boley & Durisen (2010) present numerical simulations of fragmenting gaseous disc which includes a population of dust grains and also argue for grain sedimentation inside the giant planet embryos. While we have so far concentrated on the internal evolution of individual giant embryos, Boley & Durisen (2010) paid more attention to the interaction of the embryos with their parent gas disc. These completely independent results can be cited as a direct support of our ideas.

9 CONCLUSIONS

We argued that gas clumps spawned by gravitational instability in massive young proto-planetary discs may be excellent sites for grain growth and sedimentation, in agreement with the ideas of Boss (1998); Boss et al. (2002). This may allow a direct gravitational collapse of the grain component of the central part of the giant planet embryo. This process spawns terrestrial mass solid cores without going through km-sized bodies (§7). It was also suggested that, similarly to the core accretion scenario of giant planet formation, there is a critical solid core mass at which the gas atmosphere around the solid core collapses to much higher densities. We suggest that this process may create metal rich giant planets with solid cores inside the massive gas clumps. In a companion Letter we show that these clumps should migrate inwards where they are disrupted by tidal and irradiative evaporation, releasing the inner planet. We believe this new hybrid scenario for planet formation is promising and should be explored further.

10 ACKNOWLEDGMENTS

The author acknowledges illuminating discussions with Seung-Hoon Cha, Richard Alexander, Phil Armitage and thanks Giuseppe Lodato for pointing out the Clarke & Lodato (2009) paper, and discussions of massive proto-stellar discs. Theoretical astrophysics research at the University of Leicester is supported by a STFC Rolling grant.

Table 1. Parameters of the simulations (see §3.6 for detail). ID: id of the simulations. The mass of the first core, $M_{\rm fc}$, is in Jupiter's masses; k_0 is the opacity coefficient in the opacity law given by equation 1; α is the power law index in that law; f_g is the grain mass fraction of the core; $t_{\rm end}$, in 10^3 years, is the duration of the simulation; $t_{\rm acc}$ is the time at which the runaway accretion on the high-Z core sets in, in units of 10^3 yrs; $M_{\rm core}$ is the core mass at $t = t_{\rm end}$; M_{c1} and M_{c2} are same but at times $t = 2 \times 10^3$ years and $t = 10^4$ years, respectively.

ID	$M_{\rm fc}$	k_0	α_d	f_g	$t_{\rm end}$	$t_{\rm acc}$ (10^3 yrs)	$M_{\rm core}$	M_{c1}	M_{c2}
M0α3	10	1	10^{-3}	0.02	31.5	9.1	21.6	~ 0	0.7
M1α3	10	0.1	10^{-3}	0.02	24	5.0	5.2	~ 0	4.0
M2α3	10	0.01	10^{-3}	0.02	10	1.9	1.0	0.2	1.0
M3α3	10	0.001	10^{-3}	0.02	1.5	–	10^{-6}	–	–
M2α2	10	0.01	10^{-2}	0.02	7.2	3.0	0.08	10^{-6}	0.08
M2α4	10	0.01	10^{-4}	0.02	6.4	1.8	0.7	0.12	0.7
H0α3	20	1	10^{-3}	0.02	30.	12.5	12.2	3×10^{-5}	0.0015
H1α3	20	0.1	10^{-3}	0.02	10.5	5.2	1.5	2.8×10^{-5}	1.5
H2α3	20	0.01	10^{-3}	0.02	3.	–	10^{-6}	10^{-6}	10^{-6}
H3α3	20	0.001	10^{-3}	0.02	3.	–	~ 0	~ 0	~ 0
L0α3	5	1	10^{-3}	0.02	39.7	~ 9.0	10.8	2×10^{-5}	0.15
L1α3	5	0.1	10^{-3}	0.02	20.	6.5	10.8	1.5×10^{-5}	3.4
L2α3	5	0.01	10^{-3}	0.02	32	2.4	6.2	6×10^{-5}	6.1
L3α3	5	0.001	10^{-3}	0.02	2.2	0.7	1.2	1.2	1.2
L0α1	5	1	0.1	0.02	135	NA	0.075	2×10^{-5}	10^{-4}
L0α2	5	1	0.01	0.02	46	NA	0.005	2×10^{-5}	3×10^{-4}
L1α4	5	0.1	10^{-4}	0.02	22.	5.2	10.8	5×10^{-6}	4.4
L2α2	5	0.01	0.01	0.02	14.4	4.2	3.1	2.2×10^{-5}	2.9

REFERENCES

Armitage P. J., 2007, ApJ, 665, 1381

Armitage P. J., 2010, Astrophysics of Planet Formation

Baraffe I., Chabrier G., Barman T., 2010, Reports on Progress in Physics, 73, 1, 016901

Blum J., Wurm G., 2008, ARA&A, 46, 21

Boley A. C., Durisen R. H., 2010, ArXiv e-prints

Boley A. C., Hayfield T., Mayer L., Durisen R. H., 2010, Icarus, 207, 509

Boss A. P., 1997, Science, 276, 1836

Boss A. P., 1998, ApJ, 503, 923

Boss A. P., Wetherill G. W., Haghighipour N., 2002, Icarus, 156, 291

Clarke C. J., Lodato G., 2009, MNRAS, 398, L6

Cuzzi J. N., Hogan R. C., Shariff K., 2008, ApJ, 687, 1432

Dominik C., Tielens A. G. G. M., 1997, ApJ, 480, 647

Fromang S., Papaloizou J., 2006, A&A, 452, 751

Gammie C. F., 2001, ApJ, 553, 174

Goldreich P., Tremaine S., 1980, ApJ, 241, 425

Goldreich P., Ward W. R., 1973, ApJ, 183, 1051

Helled R., Podolak M., Kovetz A., 2008, Icarus, 195, 863

Helled R., Schubert G., 2008, Icarus, 198, 156

Ida S., Lin D. N. C., 2008, ApJ, 685, 584

Inutsuka S., Machida M. N., Matsumoto T., 2009, ArXiv e-prints

Johansen A., Oishi J. S., Low M., Klahr H., Henning T., Youdin A., 2007, Nature, 448, 1022

Kippenhahn R., Weigert A., 1990, Stellar Structure and Evolution

Larson R. B., 1969, MNRAS, 145, 271

Levin Y., 2007, MNRAS, 374, 515

Low C., Lynden-Bell D., 1976, MNRAS, 176, 367

Machida M. N., Inutsuka S., Matsumoto T., 2010, ArXiv e-prints

Masunaga H., Inutsuka S., 1999, ApJ, 510, 822

Masunaga H., Inutsuka S.-i., 2000, ApJ, 531, 350

Masunaga H., Miyama S. M., Inutsuka S.-I., 1998, ApJ, 495, 346

Mizuno H., 1980, Progress of Theoretical Physics, 64, 544

Morbidelli A., Bottke W. F., Nesvorný D., Levison H. F., 2009, Icarus, 204, 558

Pollack J. B., Hubickyj O., Bodenheimer P., Lissauer J. J., Podolak M., Greenzweig Y., 1996, Icarus, 124, 62

Rafikov R. R., 2005, ApJL, 621, L69

Rees M. J., 1976, MNRAS, 176, 483

Rice W. K. M., Lodato G., Armitage P. J., 2005, MNRAS, 364, L56

Rice W. K. M., Lodato G., Pringle J. E., Armitage P. J., Bonnell I. A., 2004, MNRAS, 355, 543

Rice W. K. M., Mayo J. H., Armitage P. J., 2010, MNRAS, 402, 1740
Safronov V. S., 1969, Evoliutsiia doplanetnogo oblaka.
Sasaki S., 1989, A&A, 215, 177
Stamatellos D., Whitworth A. P., 2008, A&A, 480, 879
Stevenson D. J., 1982, P&SS, 30, 755
Toomre A., 1964, ApJ, 139, 1217
Weidenschilling S. J., 1977a, MNRAS, 180, 57
Weidenschilling S. J., 1977b, Ap&SS, 51, 153
Weidenschilling S. J., 1980, Icarus, 44, 172
Wetherill G. W., 1990, Annual Review of Earth and Planetary Sciences, 18, 205
Whitworth A. P., Zinnecker H., 2004, A&A, 427, 299
Wuchterl G., Guillot T., Lissauer J. J., 2000, Protostars and Planets IV, 1081–+
Youdin A. N., Goodman J., 2005, ApJ, 620, 459